Genome Medicine

RESEARCH

Open Access

Identification of pathological pathways centered on circRNA dysregulation in association with irreversible progression of Alzheimer's disease

Feng Wang[1†], Yangping Li[1†], Huifeng Shen[1], Paula Martinez-Feduchi[1], Xingyu Ji[2], Peng Teng[2], Siddharth Krishnakumar[1], Jian Hu[1], Li Chen[3], Yue Feng[2*] and Bing Yao[1*]

Abstract

Background Circular RNAs (circRNAs) are highly stable regulators, often accumulated in mammalian brains and thought to serve as "memory molecules" that govern the long process of aging. Mounting evidence demonstrated circRNA dysregulation in the brains of Alzheimer's disease (AD) patients. However, whether and how circRNA dysregulation underlies AD progression remains unexplored.

Methods We combined Poly(A)-tailing/RNase R digestion experimental approach with CARP, our published computational framework using pseudo-reference alignment for more sensitive and accurate circRNA detection to identify genome-wide circRNA dysregulation and their downstream pathways in the 5xFAD mouse cerebral cortex between 5 and 7 months of age, a critical window marks the transition from reversible to irreversible pathogenic progression. Dysregulated circRNAs and pathways associated with disease progression in 5xFAD cortex were systematically compared with circRNAs affected in postmortem subcortical areas of a large human AD cohort. A top-ranked circRNA conserved and commonly affected in AD patients and 5xFAD mice was depleted in cultured cells to examine AD-relevant molecular and cellular changes.

Results We discovered genome-wide circRNA alterations specifically in 5xFAD cortex associated with AD progression, many of which are commonly dysregulated in the subcortical areas of AD patients. Among these circRNAs, circGigyf2 is highly conserved and showed the highest net reduction specifically in the 7-month 5xFAD cortex. CircGIGYF2 level in AD patients' cortices negatively correlated with dementia severity. Mechanistically, we found multiple AD-affected splicing factors that are essential for circGigyf2 biogenesis. Functionally, we identified and experimentally validated the conserved roles of circGigyf2 in sponging AD-relevant miRNAs and AD-associated RNA binding proteins (RBPs), including the cleavage and polyadenylation factor 6 (CPSF6). Moreover, circGigyf2 downregulation in AD promoted silencing activities of its sponged miRNAs and enhanced polyadenylation site processing efficiency of CPSF6 targets. Furthermore, circGigyf2 depletion in a mouse neuronal cell line dysregulated circGigyf2-miRNA and circGigyf2-CPSF6

[†]Feng Wang and Yangping Li contributed equally to this work.

*Correspondence:
Yue Feng
yfeng@emory.edu
Bing Yao
bing.yao@emory.edu
Full list of author information is available at the end of the article

axes and potentiated apoptotic responses upon insults, which strongly support the causative roles of circGigyf2 deficiency in AD neurodegeneration.

Conclusions Together, our results unveiled brain circRNAs associated with irreversible disease progression in an AD mouse model that is also affected in AD patients and identified novel molecular mechanisms underlying the dysregulation of conserved circRNA pathways contributing to AD pathogenesis.

Keywords ncRNA, circRNA, miRNA, RNA-binding protein, Neurodegeneration, Alzheimer's disease

Background

Alzheimer's disease (AD) is an age-dependent neurodegenerative cortical dementia characterized by progressive cognitive impairment along with neuronal loss [1–3]. The complex etiology of AD combines multiple genetic and environmental factors, which affect broad gene networks along disease progression [4]. Over the past decades, mounting efforts have focused on identifying and understanding the causal impacts of coding gene risk factors in AD pathogenesis [5], represented by *APP*, *PSEN1/2*, and *APOE* that serve as main therapeutic targets [6–8]. However, the contributions of regulatory non-coding RNAs (ncRNAs), including small and long ncRNAs known to govern the expression of broad gene networks, have been increasingly appreciated in AD pathogenesis [9–11]. Among the distinct classes of ncRNAs, dysregulation of microRNAs (miRNAs) in AD patients' brains is well-documented, which is thought to play important roles in AD pathogenesis through regulating translation and/or stability of their target mRNAs [12, 13]. In contrast, the etiological landscape and downstream gene networks of long noncoding RNAs that govern gene expression via complex mechanisms distinct from that by miRNAs remain largely undefined. Of particular interest is circular RNA (circRNA), which plays multifaceted roles in post-transcriptional regulation and is thought to exert long-term impacts on broad gene networks in the pathogenesis of neurodegenerative diseases [14, 15].

CircRNAs are a class of single-stranded RNAs with a closed loop structure ranging from around 100 bp to over 4 kb derived from "back-splicing" [16]. Growing numbers of high-throughput transcriptomic analyses have aided in the establishment of widespread circRNA expression profiles in metazoans [17, 18], with most circRNAs enriched or specifically expressed in the brain. Compelling evidence indicated the roles of circRNAs in modulating post-transcriptional gene expression via sequestration of miRNAs and RNA binding proteins (RBPs) [16–19], which in turn regulate broad downstream biological processes that govern normal neurodevelopment [20], synaptic functions [21], and the aging process [22]. The circRNA abnormalities found in various neurological and neurodegenerative disorders [14, 23–25] strongly suggest their roles in the pathogenesis and/or progression of these diseases. Mechanistically, various RBP splicing factors bind to the flanking introns of circRNAs to modulate their biogenesis [25, 26], whose malfunction collectively underlies the dysregulation of the circRNA landscape in diseased brains.

The circularized nature of circRNAs results in their resistance to exoribonucleases, enabling them to accumulate in the brain during aging [27]. In the cerebral cortex of the elderly mice, circRNAs are proposed to serve as "memory molecules" that encode information for cognitive function [28, 29]. Hence, dysregulation of circRNAs has long been postulated as a contributing factor for aging-related cognitive disorders, represented by AD. Indeed, several publications exploited the data sets collected from a large AD cohort from the Mount Sinai Brain Bank (MSBB) to evaluate genome-wide circRNA profile changes in multiple postmortem subcortical areas, whose atrophy is most strongly correlated with cognitive decline [14, 24, 30, 31]. However, these human brain samples represent the end point of the disease. Hence, whether and how dysregulation of these cortical circRNAs contributes to AD pathogenesis and/or accelerates disease progression remains elusive. Moreover, molecular mechanisms underlying circRNA dysregulation and the functional consequences of circRNA abnormalities that lead to the formation of pathological networks that contribute to AD pathogenesis are largely undefined.

Given the facts that circRNAs harbor conserved exons and potentially shared functions between human and mouse [20, 32], we set out to explore circRNA dysregulation associated with AD pathogenic progression in the 5xFAD genetic mouse model, which expresses human *APP* and *PSEN1* that carry five AD-associated mutations with well-characterized phenotypic onset time [33–36]. Using A-tailing (poly(A)-tailing/RNase R digestion) [37] coupled with our recently published computational algorithm CARP (CircRNA identification using A-tailing RNase R approach and Pseudo- reference alignment) [38], we systematically characterized circRNA landscape alterations associated with pathogenic progression of AD in the 5xFAD cerebral cortex. We specifically focused on the 5 and 7 months of age, a critical window that marks the transition from early reversible pathology to irreversible phenotypic manifestation of AD [33, 35]. Hundreds

of circRNAs displayed dysregulation specifically associated with the rapid phenotypic progression; many are also affected in AD patients in brain region-specific manners. In addition, we discovered corrupted cooperation between many circRNAs and aberrant circRNA isoform switching, which led to dysregulation of miRNA silencing activity on their mRNA targets. Among the disease progression-associated circRNAs identified in the 5xFAD cortex, circGigyf2 is the most severely affected, highly conserved between mouse and human, and progressively downregulated in the postmortem brains of AD patients along with increased cognitive deterioration. Moreover, we identified AD-affected RBPs that control circGigyf2 biogenesis and AD-associated miRNAs and RBPs sponged by circGigyf2, which in turn caused disfunction of downstream pathways. Finally, we demonstrated the causative roles of circGigyf2 deficiency in altering AD-associated miRNA and RBP pathways and increased neuron apoptotic responses. These results unveiled novel pathological gene networks centered on cortical circRNA abnormalities that contribute to the pathogenesis of AD neurodegeneration.

Methods

Animals and cell line

5xFAD mice and age-matched control wild-type littermates were obtained from the Jackson Laboratory (wild type: C57BL/6 J 000664; 5xFAD: C57BL/6 J 5xFAD 034848). Cerebral cortex and hippocampus were collected at 5 and 7 months of age. All animal procedures and protocols were approved by the Emory University Institutional Animal Care and Use Committee (Protocol ID: PROTO201800040). All mice were housed on a 12-h light–dark cycle (7 am–7 pm) with ad libitum access to food and water and controlled around 50% humidity. Pup tail biopsies were performed at a minimum age of 12 days old for identification and genotyping. The methods of euthanasia were carried out using isoflurane anesthesia induction by open drop. Neuro-2a (N2a) cells were cultured using the standard protocol from ATCC (CCL-131). CAD (Cath.-a-differentiated) cells were maintained as described previously [39].

siRNA-mediated knockdown of RNA binding proteins and circRNA

siRNAs were designed using GenScript online tool (https://www.genscript.com/tools/sirna-target-finder) and transfections were performed using Lipofectamine 2000 Reagent (Invitrogen, 11,668,019) according to the manufacturer's protocol. To knockdown RNA-binding proteins (RBPs) important for circGigyf2 biogenesis, N2a cells were transfected with 200 pmol hnRNPL siRNA (GCCUACGCGUUUAAAUGUA), KHSRP siRNA (GUACAGCAAGCCUGUGAGA), RBM39 siRNA (GUUGGUCACGUUACUGAAC), and negative control scramble siRNA (ACGGAACGAATTAAGACAGUU). After transfection for 48 h, RT-qPCR was performed to validate the knockdown efficiency of each RBP. To knockdown circGigyf2 in CAD cells, the siRNA (AUGUAGGCUCCGUGCUCUGUCUU) targeting circGigyf2-specific back-splice junction (BSJ) site was transfected into CAD. RT-qPCR was performed 48 h post transfection with divergent primers amplifying circGigyf2 BSJ site to evaluate the knockdown efficiency.

RNA isolation and quantification

Mouse brain cortex, hippocampus tissue samples, as well as CAD and N2a cell pellets were homogenized in 1 mL TRIzol (Invitrogen, 15,596,018) and incubated at room temperature for 5 min; 200μL chloroform was added, thoroughly mixed, incubated at room temperature for 15 min, and centrifuged at 13,000 *g* for 20 min at 4 °C. Total RNA was precipitated from 600 μL supernatant in 60 μL NaAc (3 M, pH 5.2), 4 μL glycogen (5 mg/mL), and 600 μL 100% isopropanol for at least 30 min at − 80°C; 500 ng RNA was reverse transcribed (RT) using SuperScript III First Stand Synthesis System (Invitrogen, 18,080,051) with random hexamers for downstream qPCR analysis. All RT and qPCR experiments were performed in triplicate and analyzed using the relative quantification (ΔΔCt) method with *Actin* or *Gapdh* as the normalization control. All tested primers are provided in Additional File 1: Table S1. To quantify circRNA levels, divergent primers were designed to span the circRNA back splice junction (BSJ) specifically amplifying the circRNAs and not the counterpart linear RNA.

Poly(A)-tailing coupled with RNase R treatment (A-tailing)

The A-tailing/RNase R approach was described in a recent publication [37]. Briefly, 4 μL *E. coli* Poly(A) polymerase I (E-PAP) and 40U RNase inhibitor were added to 10 μg total RNA in a 50 μL reaction following the poly(A) tailing kit (Invitrogen, AM1350). The reactions were incubated for 1 h at 37 °C, purified using the RNA Clean & Concentrator-25 kit (Zymo Research, R1018), and eluted with 25 μL nuclease-free water. For RNase R treatment, the RNA products were treated with 10 U RNase R, 3 μL 10×RNase R Buffer with LiCl solution (0.2 M Tris–HCl pH 8.0, 1 mM $MgCl_2$, and 1 M LiCl), and 80U RiboLock RNase Inhibitor (40 U/μL, Thermo Fisher Scientific, EO0382) as published [37]. The RNA products were purified using the RNA Clean & Concentrator-25 kit and eluted in 30 μL nuclease-free water.

Library preparation and rRNA-depleted RNA-seq

A-tailing RNA was quantified by Qubit RNA High Sensitivity Assay (Thermo Fisher Scientific) and quality was determined by Bioanalyzer 2100 Eukaryote Total RNA Pico (Agilent Technologies). rRNA-depleted RNA-seq libraries were generated according to previously described protocols [40]. Briefly, the Ribo-Zero rRNA Removal Kit was used to deplete ribosomal RNAs. Libraries were constructed using the NEBNext UltraTM RNA Library Prep Kit according to the manufacturer's instructions. Library quality and concentrations were assessed by Tapestation High Sensitivity D1000 ScreenTapes (Agilent Technologies, 5067–5584) and qPCR, respectively. Libraries were equimolarly pooled and sequenced on the Hiseq platform with 150 PE/read length and a target of 80 M total reads (40 M in each direction) per sample (Admera Health LLC).

CircRNA identification and characterization using CARP

CircRNAs were identified and quantified using pseudo-reference annotated reads from A-tailing libraries by CARP [38]. First, candidate circRNA identification was performed by applying four different algorithms with default parameters (CIRCexplorer2, CIRI-quant, find_circ, and MapSplice) on A-tailing RNA-seq reads. Candidate circRNAs identified in each sample were then pooled and "CARP PseudoRef" was utilized to construct a pseudo-reference covering 149 bp of the flanking BSJ site for each candidate circRNA. RNA-seq reads were aligned to the pseudo-reference to detect candidate BSJ reads by "CARP Mapping." "CARP Remap" was used to detect and filter out false reads that could also be mapped to the genome or transcriptome. The remaining reads were used for circRNA quantification by "CARP ReadsCount." To determine if the circRNA was enriched in the A-tailing library, the ratio of the reads count in the A-tailing library to the control library was calculated. Expression of the last exon was calculated to represent linear RNA expression by CARP. The ratio of the last exon of the host gene, which does not form a circRNA, was also calculated for comparison by CARP. To remove circRNAs that are sensitive to A-tailing/RNase R treatment, a cutoff was set for A-tailing/control ratio for the last exons > 95%. CircRNAs with A-tailing/control ratios higher than the cutoff were considered *Bona fide* circRNAs while those with ratios lower than the cutoff were considered false positives and removed, guaranteeing an FDR < 0.05.

Differential analysis of circRNAs and circRNA clusters

CircRNA expression was quantified in triplicates for each group and normalized using the A-tailing and control libraries as described in our recent publication [38] using the following formula:

Normalized reads count for each circRNA obtained by "CARP ReadsCount" were used for differential expression (DE) circRNA analysis by *Z*-test approached used in our published circMeta algorithm[41]. Significant DE circRNAs were defined by FDR < 0.05. CircRNAs with significant changes in expression in 7-month 5xFAD mice were used to create a heatmap of their expression changes at 5 and 7 months using an in-house R script.

CircRNA clusters were defined as circRNAs sharing one common BSJ site, including the alternative 3' back splicing (A3BS) and the alternative 5' back splicing (A5BS) clusters, by "CircCluster." CircRNA cluster expression was calculated by cumulating the pseudo-reference mapped reads count of all circRNAs in that cluster and normalizing it to the A-tailing and control libraries. Normalized reads count for each circRNA cluster were used for DE analysis by *Z*-test with FDR < 0.05. Isoform proportions in each cluster were calculated based on dividing isoform-specific BSJ reads by total cluster BSJ reads. Dominant isoform was defined as the isoform of the highest abundance in that cluster.

CircRNA full-length annotation and functional prediction

CircRNA full-length was determined by "CARP CircAS" using A-tailing RNA-seq data. Junction reads in the circRNA body were summarized and *Z*-test was used for circRNA isoform switch detection using $P < 0.05$ and |Inclusion level difference| > 20% as cutoff. Using "CARP CircNetwork," miRNA binding was predicted by TargetScan based on circRNA full length determined by "CARP CircAS." miRNA soaking capacity by each circRNA was calculated by the following equation considering both circRNA abundance and number of miRNA binding sites in each circRNA molecule:

$$\text{Soaking Capacity} = \text{circRNA expression} \times \sum_{i=1}^{n} \left(\text{logistic probability of ith binding site}\right)$$

To evaluate the changes in miRNA activity, $\log_2$ fold change of top 10% targets defined by weighted context + + score predicted by TargetScan was compared to $\log_2$ fold change of non-miRNA targets. *t*-test with $P < 0.05$ was used to determine if there was a significant difference between miRNA top targets and non-miRNA targets, which indicates changes in miRNA activities.

CircRNA-RBP bindings were predicted by "CARP CircRBP" with integrated machine learning algorithm CRIP

[42]. CircGigyf2-RBP-AD risk score for each RBP are calculated based on their binding probability to circGigyf2 and their association to AD risk using the following equation:

$$\text{Risk score} = -\log_{10}^{P-\text{value[RBP targets, AD risk genes]}} \times \text{Binding Probability[circGigyf2, RBP]}$$

where the AD risk genes were defined by relevance score > 2 from GeneCards (https://www.genecards.org/Search/Keyword?queryString=AD). RBP binding for skipped exons of circCcdc50 was predicted by RBPsuite, as CRIP is unable to analyze short fragments [43].

Validation of cassette exon exclusion in circCcdc50

RNA products were treated using the A-tailing/RNase R approach as described above and then eluted in 30 µL nuclease-free water using the RNA Clean & Concentrator-25 kit; 8 µL cleaned RNA were reverse transcribed (RT) and performed qPCR experiments following the above described. The primers were designed to span the junction site specifically in isoforms with cassette exon inclusion and exclusion of circCcdc50 (Additional File 1: Table S1).

Predict RBP binding to circRNA flanking introns

NCBI37/mm9 mouse genome assembly gene structure annotation and sequence extraction by "bedtools getfasta" were used to determine DE circRNAs flanking introns. 137 RBPs' binding probabilities were predicted by CRIP (CircRNAs Interact with Proteins) for the flanking introns based on their sequence [42]. Only RBPs located in the nucleus were considered as candidate circRNA biogenesis regulators [44].

Expression analysis for mRNAs

Sequencing reads from the control library were aligned to mm9 by TopHat 2.1.0 [45] using default parameters. Aligned bam files were used for DE genes between 5xFAD and CTL at each time point using Cuffdiff [46]. DE genes were defined by q-value < 0.05. GO analysis for DE genes was performed using Protein Annotation Through Evolutionary Relationship (PANTHER) [47]. RNA-seq data for CPSF6 overexpression was downloaded from Gene Expression Omnibus (GSE179630) [48] to identify CPSF6 targets.

CircRNA-miRNA pull-down assay

Biotinylated circGigyf2 probe (/5Biosg/CACTGGACAGAGCACGGAGCCTACATCTTT) and the scramble control probe (/5Biosg/AGCCTCGGTTAACGTGATGATGCGAGCTAA) were synthesized by Integrated DNA Technologies, Inc. Mouse brain cortex samples were digested in lysis buffer (NaCl 150 mM, Tris–Cl 25 mM, pH-7.5, DTT 5 mM, 0.5% IGEPAL, 60 U/mL SUPERase In RNase Inhibitor (Invitrogen, AM2696), and 1 × Protease Inhibitor (Roche, 04693116001) at 4°C for 2 h with rotation. Following centrifugation at 12,000 *g* for 10 min at 4 °C, 10% volume of cleared lysates was removed as input. The rest of the cleared lysates (90%) were incubated with 8 µg biotinylated probe and rotated at 4 °C overnight. The next day, 75 µL streptavidin C1 magnetic beads (Invitrogen, 65,002) were mixed with probe-lysate solution and rotated for 3 h at 4 °C. The beads were washed three times with wash buffer (KCl 10 mM, MgCl2 1.5 mM, Tris–Cl 10 mM pH 7.5, DTT 5 mM, NaCl1 M, 0.5% NP-40, 60U/ mL SUPERase In RNase Inhibitor, and 1 × Protease Inhibitor), each time being vortexed 15 s and incubated 1 min at room temperature. The beads were resuspended in 300 µL nuclease-free water, vortexed for 15 s and incubated 95 °C for 5 min. The beads were placed on a magnetic rack for 5 min, and 300 µL supernatant were transferred to new tubes with equal volume phenol:chloroform:isoamyl alcohol (25:24:1, pH 6.8). RNA was precipitated in 30 µL NaAc (3 M, pH 5.2), 2 µL glycogen (5 mg/mL), and 300 µL 100% isopropanol overnight at − 80°C. RNA pellets were collected by centrifugation at 20,000 *g* for 20 min and washed with 75% ethanol. The same volume RNA was reverse transcribed (RT) into cDNA with random hexamers for circGigyf2 pull-down efficiency analysis. All RT and qPCR experiments were performed in triplicate and analyzed using the ΔΔCt method with circRNA expression input as the normalization control. All RT-qPCR primers are provided in Additional File 1: Table S1.

Quantitative detection of miRNAs

RT-qPCR quantification of miRNAs was performed using TaqMan Advanced miRNA Assay (Applied Biosystems, A28007). Briefly, 2 µL circGigyf2 pull-down RNA samples underwent poly(A) tailing with poly(A) enzyme and adapter ligation with RNA ligase and ligation adapter. The RT reaction was added to each adapter ligation reaction, and the mixtures were incubated at 42 °C for 15 min and 85 °C for 5 min; 5 µL RT reaction products were added to 45 µL miRNA-amplification (miR-Amp) reaction mix and amplified in thermocycler. TaqMan Advanced miRNAs Assays (Additional File 1: Table S1) were used to detect the binding of miRNAs to circGigyf2 by RT-qPCR utilizing a 1:10 dilution of cDNA template (miR-Amp reaction products). The relative quantification

(ΔΔCt) method was used with miRNA expression input as the normalization control.

CircRNA-RBP pull-down assay

Mouse brain cortex samples were digested in cold lysis buffer (150 mM NaCl, 10 mM Tris–Cl pH 7.5, 1 mM EDTA, 1 mM EGTA, 0.5% NP-40, 1% Triton X-100, 0.1% SDS, 60 U/mL SUPERase In RNase inhibitor, 1 × protease inhibitor) at 4 °C for 2 h with rotation. Lysates were centrifuged at 12,000 *g* for 10 min at 4 °C, and 5% volume cleared lysates were saved as input. The rest of the cleared lysates (90%) were rotated with 8 μg biotinylated probe for 4 h at 4 °C; 75 μL streptavidin C1 magnetic beads were added and rotated for 3 h at 4 °C. The beads were washed three times with cold lysis buffer, each time being vortexed 15 s and rotated for 5 min at 4 °C. The circGigyf2 pull-down RBPs were analyzed by western blot.

Changes of miRNA activity and proximal PAS processing efficiency

To investigate miRNA activity changes, conserved miRNA targets were retrieved from TargetScan database and top 10% ranked miRNA targets based on weighted context + + score were considered as confident miRNA targets [49]. Log_2 fold changes of miRNA targets and non-miRNA targets were calculated and compared by student *t*-test, miRNAs with $P < 0.05$ considered significantly activity change. Polyadenylation site (PAS) of mouse (mm9) was retrieved from PolyA_DB V3.2 and reads spanning each proximal PAS were counted by featureCounts [50, 51]. Reads were normalized to counts per million mapped reads and compared between 5xFAD and their control littermates. PAS spanning reads with $|\log_2$ fold change $> 0.5|$ were considered as increased or decreased PAS processing efficiency.

Western blot

The RBPs pulled down by circGigyf2 were boiled in 2 × Laemmli loading buffer for 9 min at 95 °C prior to western blot analysis. The following antibodies were used in this study (Additional File 2: Table S2): rabbit anti-CPSF6 (1:3000, Abcam, AB99347), mouse anti-GAPDH (1:5000, Invitrogen, AM4300), abbit anti-QKI (1:2000, ThermoFisher Scientific, A300-183A), and mouse anti-TDP43 (1:3000, Proteintech, 10,782–2-AP).

Assessment of cell apoptosis

Eighteen hours after transfection of circGigyf2 siRNA, CAD cells were treated with 25 μM C2-ceramide for 6 h as described previously [52]. TUNEL Assay Kit-BrdU-Red (Abcam, ab66110) was then used to detect cell apoptosis according to the manufacturer's instructions. The TUNEL assay images were captured by Nikon Eclipse Ti-E microscope with fluorescence BrdU-Red and DAPI. Percentage of cell apoptosis was calculated using the numbers of BrdU-Red + cells divided by the numbers of DAPI-labeled total cells.

Human postmortem brain data analysis

RNA-seq data for multiple human postmortem subcortical areas including the frontal pole (BM10, $n = 317$), superior temporal gyrus (BM22, $n = 324$), parahippocampal gyrus (BM36, $n = 311$), and inferior frontal gyrus (BM44, $n = 301$) generated from Mount Sinai Brain Bank (MSBB) cohort were downloaded from Synapse database (https://www.synapse.org/Synapse:syn7416949) [31]. CIRCexplorer2 was used to quantify circRNA expression in each sample and only circRNA expressed (Junction Reads Count > 2) in more than 30 samples were used for AD correlation analysis [38]. CircRNA expression was then correlated with AD clinical dementia rating (CDR) using DESeq2 with post-mortem interval (PMI), age of death (AOD), sex, and batch as covariates [53]. Gene expressions were quantified by featureCounts and correlated with AD CDR using DESeq2 with the same covariates [51]. PAS of human (hg19) was retrieved from PolyA_DB V3.2 and reads spanning each proximal PAS counted by featureCounts were correlated with AD CDR using DESeq2 to determine proximal PAS processing efficiency change in AD [50].

Statistics

Differential analyses of circRNAs, circRNA clusters, and circRNA isoform changes were performed by *Z*-test after normalization to A-tailing libraries and untreated libraries [38]. mRNA differential analysis was conducted by Cuffdiff [54]. DESeq2 linear regression model was used to calculate circRNA, mRNA, and proximal PAS processing efficiency changes in human postmortem brains [53]. miRNA activity changes were compared between miRNA top targets and non-miRNA targets using unpaired *t*-test. Unpaired *t*-tests were also used for comparison between two conditions for RT-qPCR, western blot quantification, and cell apoptosis quantification. Pearson correlation was used for quantitative correlation analysis. Spearman correlation was used for correlation analysis for ranked factors. Significant overlapping between gene sets was determined by exact binomial test.

Results

Identification of altered circRNA landscape in the cerebral cortex of the 5xFAD mice associated with pathological progression toward irreversible phenotypes

Mutations in *APP* and *PSEN1* have been linked to the dominant inheritance of early onset of familial AD [5]. The 5xFAD transgenic mice express human *APP* and

PSEN1 with five AD associated mutations and recapitulate major milestones of AD pathology with well-characterized phenotypic onset time [33–36], hence offering a reasonable model for studying pathological alterations of the circRNA landscape that contribute to AD pathogenesis. The 5xFAD mice show early Aβ plaque deposition in cortex and start to exhibit memory impairment when reaching 5 months of age while develop massive Aβ accumulation and severe memory defects at 7 months of age (Fig. 1A and Additional File 3: Table S3). Moreover, therapeutic treatments of 5xFAD mice at 5 months of age have been reported to prevent or ameliorate the rapid progression of AD phenotypes whereas 7 months of age denotes a therapeutically irreversible stage (Additional File 3: Table S3) [55, 56]. Thus, we explored whether and how the cortical circRNA landscape is differentially affected at 5 and 7 months of age, which may contribute to the transition toward irreversible disease progression of AD (Fig. 1A).

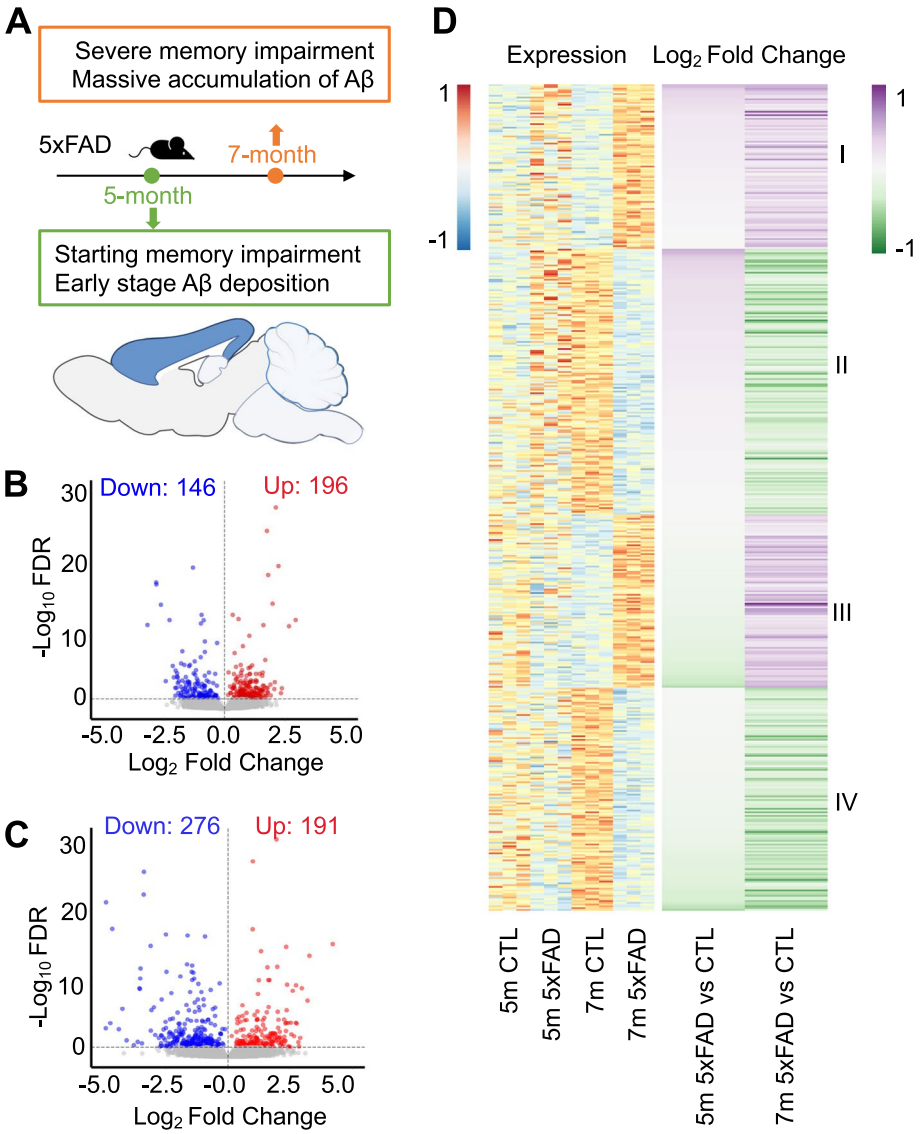

Fig. 1 Identification of circRNA landscape changes in 5xFAD mouse cortex associated with irreversible AD progression. **A** Milestone AD phenotypes in 5-month and 7-month 5xFAD mice utilized for experimental design. Mouse cerebral cortex (highlighted in blue) from 5xFAD and their littermate controls were used for circRNA analysis. **B**–**C** Downregulated (blue) and upregulated (red) circRNAs were detected in 5-month (**B**) and 7-month 5xFAD cerebral cortex (**C**) compared to their age-matched wildtype control littermates (CTL) (FDR < 0.05, *Z*-test). *X*-axis and *Y*-axis represent the $\log_2$ fold change and $-\log_{10}$FDR between 5xFAD and CTL mice. **D** Heatmaps of AD-associated circRNA expression levels (left) and $\log_2$ fold change (right) in 5-month and 7-month AD and CTL littermates

We utilized in vitro poly(A)-tailing and RNase R digestion [37] in combination with the pseudo-reference-based computational framework (A-tailing/CARP) established in our previous study [38] (Additional File 4: Fig. S1A) to determine genome-wide circRNA landscape from triplicated 5- and 7-month-old 5xFAD cerebral cortex along with their wild-type littermate controls (CTL). This method takes advantage of the resistance of circRNAs to RNase R digestion while linear transcripts are universally and completely removed (Additional File 4: Fig. S1B). The pseudo-reference was built upon candidate circRNAs identified from several algorithms based on RNA-seq reads spanning circRNA back-splice junctions [57–60]. Given the variations among these pipelines (Additional File 4: Fig. S1C) [61], CARP has been demonstrated to achieve superior sensitivity, reliability, and reproducibility for circRNA identification and quantification from A-tailing dataset [38]. As a result, full-length *bona fide* circRNAs are accurately identified and quantified, allowing us to explore their functions as molecular decoys. The last exon could not form circRNA due to the lack of downstream flanking intron. Thus, the last exon reads count ratio between libraries with and without A-tailing/RNase R treatment was used as reference to define RNAs that were sensitive or resistant to the A-tailing/RNase R process with false discovery rate (FDR) < 0.05 (Additional File 4: Fig. S1D). This helped us to filter out false-positive circRNAs that are actually sensitive to RNase R treatment [38].

We went on to perform circRNA differential expression (DE) analysis and identified 342 and 467 circRNAs that were significantly dysregulated in 5xFAD cortex at 5 or 7 months of age (FDR < 0.05, Fig. 1B, C), respectively. Of note, circRNA fold changes calculated by CARP were highly correlated with fold changes calculated by another algorithm CIRIquant (Additional File 4: Fig. S1E). Importantly, no significant changes were detected in linear transcripts derived from the same host genes that give rise to the DE circRNAs in the 7-month 5xFAD cortex (Additional File 4: Fig. S1F and Additional File 5: Table S4 and Table S5), indicating that circRNAs, but not their host genes, are specifically affected.

To identify circRNAs associated with irreversible AD progression, all DE circRNAs identified in the 7-month 5xFAD cortex compared to CTLs were further classified into four groups based on their differential trends of alterations relative to their changes at the 5 months of age (Fig. 1D and Additional File 5: Table S4). Group I DE circRNAs showed progressive increase in the 5xFAD cortex compared to CTL from 5 to 7 months of age whereas Group IV displayed a continuous decline, suggesting their progressive and accumulative roles during early AD pathological advancement. In contrast, DE circRNAs in Groups II and III showed dysregulation in opposite directions in the 5xFAD cortex at 5 and 7 months, respectively. Group II switched from a trend of increase at 5 months to downregulation at 7 months whereas Group III switched from decrease to upregulation, hence are most likely involved in stage-specific AD pathology.

To identify AD-associated circRNAs that are conserved and commonly affected in AD mice and AD patients, we systematically compared circRNA landscape changes in the 7-month-old 5xFAD cortex with DE circRNAs found in AD patients. The publicly available RNA-seq data from the Mount Sinai Brain Bank (MSBB) cohort studies derived from four different cortical areas, namely frontal pole (BM10), superior temporal gyrus (BM22), parahippocampal gyrus (BM36), and inferior frontal gyrus (BM44), were used [31]. Published circRNAs profiling in human AD entorhinal cortex from an independent cohort, which is affected in the initial stage of AD, were also included in the analysis [30]. Despite the aging-programmed circRNA landscape differences [29, 62], the mouse cortical circRNA landscape at 7 months of age showed 13.14% to 16.34% overlap with those in the above subcortical areas of the aged human cohort (Additional File 4: Fig. S2A). Hundreds of these conserved circRNAs are commonly dysregulated in both the 5xFAD mouse cortex and human postmortem subcortical areas, among which BM10, BM22, BM36, and BM44 harbor comparable percentages of upregulated (7.13–8.46%) and downregulated (12.84–14.77%) circRNAs overlapping with the total dysregulated cortical circRNAs in 7-month 5xFAD mice (Additional File 4: Fig. S2B, C). However, a markedly lower percentage of dysregulated circRNAs (2.50% upregulated and 2.04% downregulated) overlaps between AD entorhinal cortex and 7-month 5xFAD cortex (Additional File 4: Fig. S2B, C). These data suggest that conserved circRNAs dysregulated at the irreversible progression point of AD in 5xFAD cortex are also affected in AD patient brains, in a region-specific manner. Further analysis revealed that although the overall baseline circRNA expression profiles substantially overlap among the human entorhinal cortex and the BM36/44 subcortical areas (Additional File 4: Fig. S2D), AD-affected circRNAs (circRNAs changed in AD) in the entorhinal cortex are remarkably different from those affected in the BM36/44 subcortical areas, two most vulnerable cortical areas related to AD pathology (Additional File 4: Fig. S2E and F) [63].

To further explore the brain region specificity of AD-associated circRNAs, we performed circRNA DE analysis in the 7-month 5xFAD mouse hippocampus, a brain region also severely affected in AD (Additional File 4: Fig. S3A). We identified 7025 total and 264 DE circRNAs (Additional File 4: Fig. S3B, C). Although 6329 (90.09%)

circRNAs identified in 7-month mouse hippocampus are also expressed in mouse cerebral cortex (Additional File 4: Fig. S3B), only 5 (1.89%) circRNAs were commonly affected in 5xFAD cortex and hippocampus (Additional File 4: Fig. S3D, E). The distinct circRNA landscape disruption in 5xFAD cortex and hippocampus, together with the subcortical region-specific dysregulation of circRNAs in human AD patients (Additional File 4: Fig. S2), demonstrated brain-region-specific circRNA abnormalities, which may contribute to the temporospatial differences in AD pathological progression and phenotypes. To determine cell composition in 7-month-old 5xFAD and their littermates, we applied a well-established deconvolution approach CIBERSORT that can accurately infer cell-type abundance and cell-type-specific gene expression from RNA profiles of intact tissues [64], using RNA-seq from different types of brain cells isolated by immunopanning [65]. Consistent with the previous pathology studies, the output from CIBERSORT confirmed a neglectable cell proportion and abundance change (< 2%) between 7-month 5xFAD and their littermate controls, ruling out the impact of neuronal loss in circRNA landscaping (Additional File 4: Fig. S3F).

Functional cooperation by multiple AD-affected circRNAs underlie dysregulation of the miRNA-mRNA axis in the 5xFAD cortex

The number of cortical circRNAs (16,367) in CTL identified by A-tailing/CARP far exceeded the cortical circRNAs available in circBase (1770) that were mainly identified based on back splice junction (BSJ) reads from total RNA libraries without poly(A)-tailing RNase R digestion (Fig. 2A and Additional File 4: Fig. S3G) [20]. The 15,045 circRNAs detected specifically by A-tailing were expressed at significantly lower levels (BSJ reads count < 10) than the commonly detected circRNAs ($P < 2.2 \times 10^{-16}$, *t*-test), demonstrating that A-tailing/CARP is more sensitive and effective in detecting low abundance circRNAs (Fig. 2B). We next explored whether multiple distinct circRNAs, especially those low abundance circRNAs detected by A-tailing/CARP but missed by traditional circRNA detection methods, may exert concomitant effects to silence miRNAs. One miRNA, miR-122-5p, is aberrantly upregulated in the brain of AD patients [12, 66, 67]. We found a significantly cumulative reduction of miR-122-5p top mRNA targets in the 5xFAD versus WT mouse cortex at 7 months of age ($P = 0.01$) as compared to $\log_2$ fold change of mRNAs that are not targeted by miR-122-5p (Fig. 2C). Such alterations were not observed in 5-month 5xFAD cortex ($P = 0.26$, data not shown). This result revealed miR-122-5p hyperfunction upon irreversible AD progression. To explore whether and how AD-affected circRNAs may underlie miR-122-5p hyperfunction, we searched for miR-122-5p binding sites in each dysregulated circRNA in the 7-month 5xFAD cortex. Forty-five downregulated circRNAs and 30 upregulated circRNAs were identified that harbor miR-122-5p binding sites (Fig. 2D). Thus, the hyperactivity of miR-122-5p in the 5xFAD cortex likely results from the cooperation of multiple dysregulated circRNAs, among which the additive soaking effects by downregulated circRNAs apparently outweigh the impacts of the upregulated circRNAs (Fig. 2D).

Among these 35 miR-122-5p-interacting circRNAs that are downregulated and expected to contribute to miR-122-5p hyperactivity in the 5xFAD cortex, 31 were expressed at low abundance (BSJ RC < 10) and collectively contained 33 binding sites, whereas 4 high abundance circRNAs (BSJ RC > 10) together contain 5 binding sites (Fig. 2E). Using the Software for Statistical Folding of Nucleic Acids and Studies of Regulatory RNAs (Sfold) [68], the circRNA-miRNA binding probability for each site was predicted based on the RNA-interacting sequence, thermodynamics, and target structure features at the predicted miRNA binding sites [69]. We found that the miRNA-binding probability for each predicted site on the high- and low-abundance circRNAs did not differ significantly (Fig. 2F), suggesting that each of these circRNAs could contribute to the sequestration of miR-122-5p. Hence, the total capacity for soaking miR-122-5p is defined as the sum of each circRNA's soaking ability, calculated by the circRNA expression level times total miR-122-5p binding probability (see "Methods"). As a result, low-abundance circRNAs were collectively responsible for 30.62% of the total sponging capacity for miR-122-5p (Fig. 2G), which has been overlooked due to less sensitive detection methods used. The high-abundance circRNAs contributed to the remaining 69.38% soaking capacity. These results suggest that multiple circRNAs can cooperate and exert additive effects for the sequestration of a specific miRNA, and the precise circRNA regulation can be underestimated if only focusing on high abundant ones. Hence, dysregulation of circRNAs at low abundance, each displaying an unfavored stochastic ratio to a miRNA, could act collectively to make a substantial contribution in regulating the miRNA–mRNA axis in diseased brains.

CircRNA isoforms are dysregulated during pathologic progression in the 5xFAD cortex, which alter activities of bound miRNAs and RBPs and downstream mRNA targets

Multiple circRNA isoforms derived from the same host gene with various lengths but contain common sequences through alternative back splicing from the shared common 3' BSJ site are referred as circRNA clusters [17,

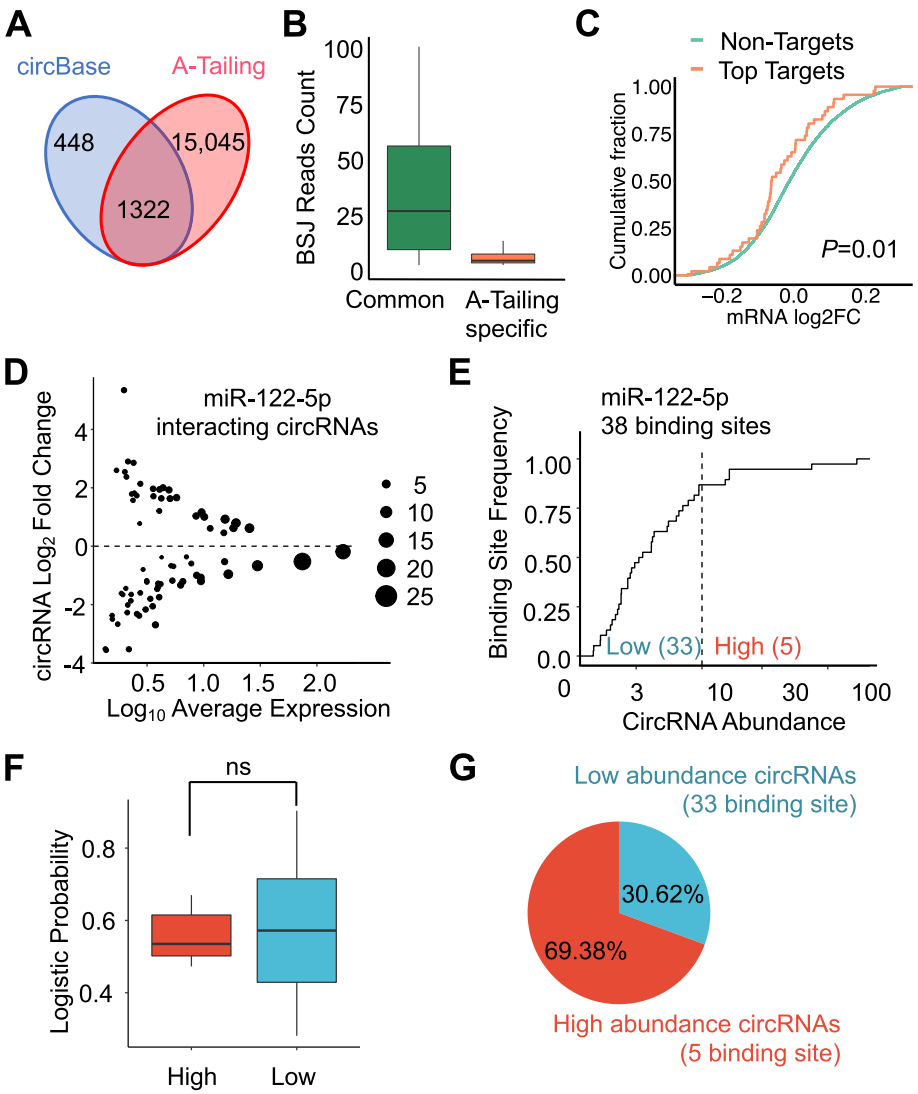

Fig. 2 Functional cooperation by multiple circRNAs in regulating AD-related miRNA activities. **A** Venn diagram comparing the mouse cortical circRNA landscape identified by A-tailing RNase R treatment in our study with circRNA profiles generated without A-tailing published in circBase. **B** Expression levels of circRNAs commonly found in A-tailing and circBase (common) and circRNAs specifically detected by A-tailing (A-tailing-specific). **C** Significant cumulative reduction of the top 10% mRNA targets (top targets, red) for miR-122-5p predicted by TargetScan ($P = 0.01$, *t*-test) in the 5xFAD cortex as compared to all mRNAs that do not contain predicted miR-122-5p sites (non-targets, green). **D** More downregulated circRNAs in the 7-month 5xFAD cortex (45) are predicted to bind miR-122-5p than upregulated circRNAs (30). Each dot represents a significant DE circRNA in 7-month 5xFAD compared to CTL. *X*-axis represents the $\log_{10}$ average expression level of each circRNA. *Y*-axis represents $\log_2$ fold change of circRNA expression in 7-month 5xFAD compared to CTL. Dot size represents the net change of abundance for each circRNA in 5xFAD compared to CTL. **E** Among all downregulated circRNAs, 33 of 38 miR-122-5p binding sites belong to low abundance circRNAs, defined by normalized reads count < 10. **F** The predicted logistic binding probability for each miR-122-5p site in high- and low-abundance DE circRNAs in the 7-month 5xFAD cortex is not significantly different. **G.-** Binding capacity for miR-122-5p by high-abundance and low-abundance DE circRNAs identified in the 7-month 5xFAD cortex. miR-122-5p binding capacity by each circRNA was calculated by circRNA net change of abundance, number of miR-122-5p binding sites (*n*), and logistic probability for each binding site

19]. We identified 440 significant DE circRNA clusters in 7-month 5xFAD cortex compared to CTLs (Fig. 3A). Nearly half (212 out of 440) of the significant DE circRNA clusters did not harbor any significant DE individual circRNAs identified in Fig. 1C. The expression of each circRNA within a given cluster is usually a fraction of the overall expression of that cluster. Therefore, many individual circRNAs in a cluster might not reach statistical significance in DE analysis, but circRNAs within the cluster can work together as a group. The function of these clustered circRNAs will be overlooked if only AD-associated individual circRNAs were examined. Among

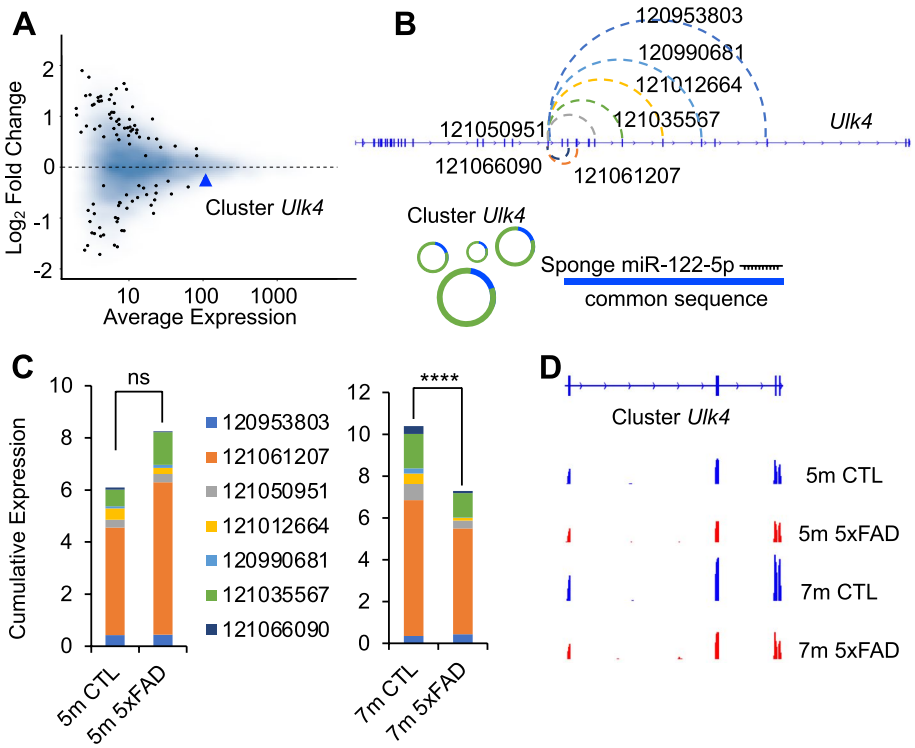

Fig. 3 Dysregulation of circRNA clusters associated with AD progression. **A** Differentially expressed (DE) circRNA clusters derived from alternative 3′ back splicing in 7-month 5xFAD mice. Blue background represents all circRNA clusters in 7-month CTL and 5xFAD mice. Black dots indicate DE circRNA clusters (FDR < 0.05, *Z*-test) that do not carry significantly altered individual circRNA component. *X*-axis indicates the average expression of each cluster in the cortex. *Y*-axis indicates $\log_2$ fold change of the cluster expression in the 7-month 5xFAD cortex compared to CTL. CircRNA cluster *Ulk4* is highlighted by a blue triangle. **B** Schematic of the circRNA cluster *Ulk4*, including seven circRNAs that share a common 3′ back splicing site. The genomic coordinates of the 5′ back splicing sites for each circRNA are indicated. **C** Cumulative expression levels of the *Ulk4* circRNA cluster with stacked expression levels for each circRNA component in 5xFAD and CTL in 5-month (left) and 7-month (right) cortex (****$P < 0.0001$). **D** IGV views show that the common sequence of the *Ulk4* circRNA cluster is specifically downregulated in 7-month, but not 5-month, cortex of 5xFAD compared to CTL

them, the *Ulk4* circRNA cluster, which contains seven non-significantly changed circRNA isoforms (Fig. 3B), became significantly downregulated in 7-month 5xFAD cortex but not affected at 5-month of age (Fig. 3C, D). The common sequence of the *Ulk4* circRNA cluster was predicted to bind the AD-associated miR-122-5p (Fig. 3B). Hence, deficiency of the Ulk4 circRNA cluster, together with multiple individual DE circRNAs (Fig. 2E), collaboratively contribute to miR-122-5p hyperactivity observed in the 7-month 5xFAD cortex (Fig. 2C). To our knowledge, this is the first example for additive effects by circRNAs within a cluster that fine-tune the activities of AD-related miRNAs.

CircRNA isoforms are also derived from alternative splicing (AS) of cassette exons within the circRNA body, leading to altered function [38, 70]. Taking advantage of A-tailing RNase R treatment that eliminates linear RNAs therefore allowing direct reads map to full-length circRNA-forming exons in addition to BSJs, we identified 156 circRNAs that harbor aberrant alternative exon inclusion in 7-month 5xFAD cortex compared to CTLs (Fig. 4A). The switch between the long and short circRNA AS isoforms are predicted to regulate their sponging abilities for miRNAs and RBPs [38]. One example is the inclusion/exclusion of a cassette exon (exon 4 of NM_001289436, chr16:27,407,107–27407152, NCBI37/mm9 Mouse Assembly) in circCcdc50, which was dysregulated upon irreversible pathological progression in 5xFAD cortex (Fig. 4B–E). The inclusion of exon 4 in circCcdc50 was comparable between CTL (39.08%) and 5xFAD (32.99%) at 5 months of age (Fig. 4B and D). However, at 7 months of age, while exon 4 inclusion rate in circCcdc50 remained the same in CTL (39.47%), a marked reduction was observed in of 7-month 5xFAD cortex (5.26%) (Fig. 4C and E). The reduced inclusion was also detected in 5xFAD hippocampus (41% in WT, 37% in 5xFAD). This AS event was specific for circCcdc50, as it could not be detected in host gene mRNAs (Additional File 4: Fig. S4A). RT-qPCR using circCcdc50 isoform-specific primers (Additional File 4: Fig. S4B) further

confirmed reduced inclusion along with increased exclusion exon 4 in 7-month 5xFAD cortex (Additional File 4: Fig. S4C).

CircRNA isoform switching could alter interaction with miRNAs or RBPs [70, 71]. Seven miRNAs are predicted to bind exon 4 in circCcdc50 (Fig. 4F), among which miR-335-5p is associated with aberrant gene expression in AD postmortem brains [72]. Skipping exon 4 in circCcdc50 in the 7-month 5xFAD cortex led to a significant cumulative reduction of miR-335-5p mRNA targets, consistent with the release of miR-335-5p (Fig. 4G). Moreover, using the deep learning-based algorithm RBPsuite [43], several RBPs were predicted to bind exon 4 in circCcdc50 (Fig. 4H). Among these RBPs, trinucleotide repeat containing adaptor 6A (TNRC6) is a core protein in an RNA-induced silencing complex, whose availability controls global miRNA activities [73]. We performed a systematic survey for each mouse miRNA in TargetScan to examine the cumulative effects on dysregulation of mRNA targets in 7-month 5xFAD. Remarkably, an ectopic boosting of global miRNA activities was observed (Fig. 4I), consistent with the release of the sponged TNRC6 due to exon 4 skipping in circCcdc50 [74]. These data suggest that dysregulation of alternative exon inclusion in circRNAs could alter their sponging activity, which could contribute to the abnormal activity of many miRNAs upon AD progression.

Adenine to inosine (A-to-I) editing has been suggested to affect circRNA functionality and translatability [75, 76]. Using a published algorithm, Software for Accurately Identifying Locations Of RNA-editing (SAILOR), we assessed adenosine to inosine changes from the untreated and A-tailing treated RNA-seq data. A unique advantage of our A-tailing and untreated control (no RNase R treatment to remove linear RNAs) data is that we can quantify A-to-I editing level specifically in circRNAs enriching A-tailing library where linear RNAs were completed removed, meanwhile quantifying A-to-I editing level in none circRNA regions using untreated library where linear RNAs are much more abundant. Among the 9500 A-to-I editing site obtained in A-tailing/RNase R treated AD and controls, we identified 1176 transcriptome-wide A-to-I editing changes in 5xFAD cortex ($P < 0.05$, A-to-I editing level change > 10% in either 7-month 5xFAD or their littermate controls). While the gain- or loss of A-to-I editing on linear RNA transcripts from AD mice were roughly equal (Additional File 4: Fig. S4D, left bar), we found significantly enhanced A-to-I editing in the circRNA pool (653) than loss of A-to-I editing (373) ($P = 0.0078$) (Additional File 4: Fig. S4D, right bar), which is consistent with the increased A-to-I editing in circRNA that has been observed in human AD entorhinal cortex [77].

CircGigyf2 is downregulated in specific brain regions of 5xFAD mice and AD patients along disease progression and its biogenesis requires multiple RBPs that are critical for brain function.

Among the circRNAs specifically dysregulated in the 7-month 5xFAD cortex identified by A-tailing/CARP (Fig. 5A), circGigyf2 was the most abundantly expressed and severely downregulated (Fig. 5A, B). The downregulation of circGigyf2 was further validated by RT-qPCR using a primer set specifically spanning its BSJ site. Importantly, circGigyf2 was unchanged at 5 months (Fig. 5C) but significantly downregulated at 7 months in the 5xFAD cortex (Fig. 5D), indicating that circGigyf2 deficiency occurs upon irreversible progression of AD. In contrast, the linear *Gigyf2* mRNA level was not altered in 5xFAD at either 5 or 7 months of age (Additional file 4: Fig. S5A). Interestingly, no significant changes of circGigyf2 were observed in 7-month 5xFAD hippocampus (Additional file 4: Fig. S5B), suggesting that circGigyf2 deficiency in AD is brain-region-specific.

The organization of circRNA-forming exons in the murine and human host gene *Gigyf2/GIGYF2* and the

(See figure on next page.)

Fig. 4 Altered exon inclusion within circRNA isoforms leads to dysregulated activities of miRNAs and RBPs during AD progression. **A** Volcano plot of global circRNA isoform switching due to alternative inclusion of internal exons was identified by A-tailing/CARP in 7-month 5xFAD mice. Isoform switching events are classified as short-to-long (red) and long-to-short (blue), due to the inclusion or skipping of cassette exons within circRNAs. **B**–**C** The inclusion level of exon 4 (red) in circCcdc50 in the cortex of 5-month (**B**) and 7-month (**C**) 5xFAD and CTL. Junction read counts (JRC) are in red if they support exon inclusion and in green if they support exon skipping. Exon inclusion level = Average of exon inclusion JRC / (Average of exon inclusion JRC + exon skipping JRC). **D**–**E** IGV views confirm that the cassette exon within circCcdc50 (highlighted by dotted red box) is present in both 5xFAD and CTL cortex at the 5 months of age (**D**) but is skipped at 7 months of age in 5xFAD cortex (**E**). **F** Putative miRNAs sponged by the constitutive exons and the cassette exon of circCcdc50. Seven miRNAs predicted for exclusive interaction with the cassette exon are listed, including miR-335-5p (bold). **G** Significant downregulation of the top 10% mRNA targets for miR-335-5p (red) predicted by TargetScan compared with non-target genes (****$P = 6.64 \times 10^{-5}$, *t*-test). **H** RBPs predicted to bind circCcdc50's cassette exon and constitutive exons. The six RBPs predicted to bind only to the cassette exon are listed. **I** The silencing activity of most miRNAs indicated in this panel is significantly strengthened (*X*-value < 0) in 7-month 5xFAD cortex (red, $P < 0.05$). *X*-axis represents the difference of the mean $\log_2$ fold change between the miRNA targets and non-miRNA-targets

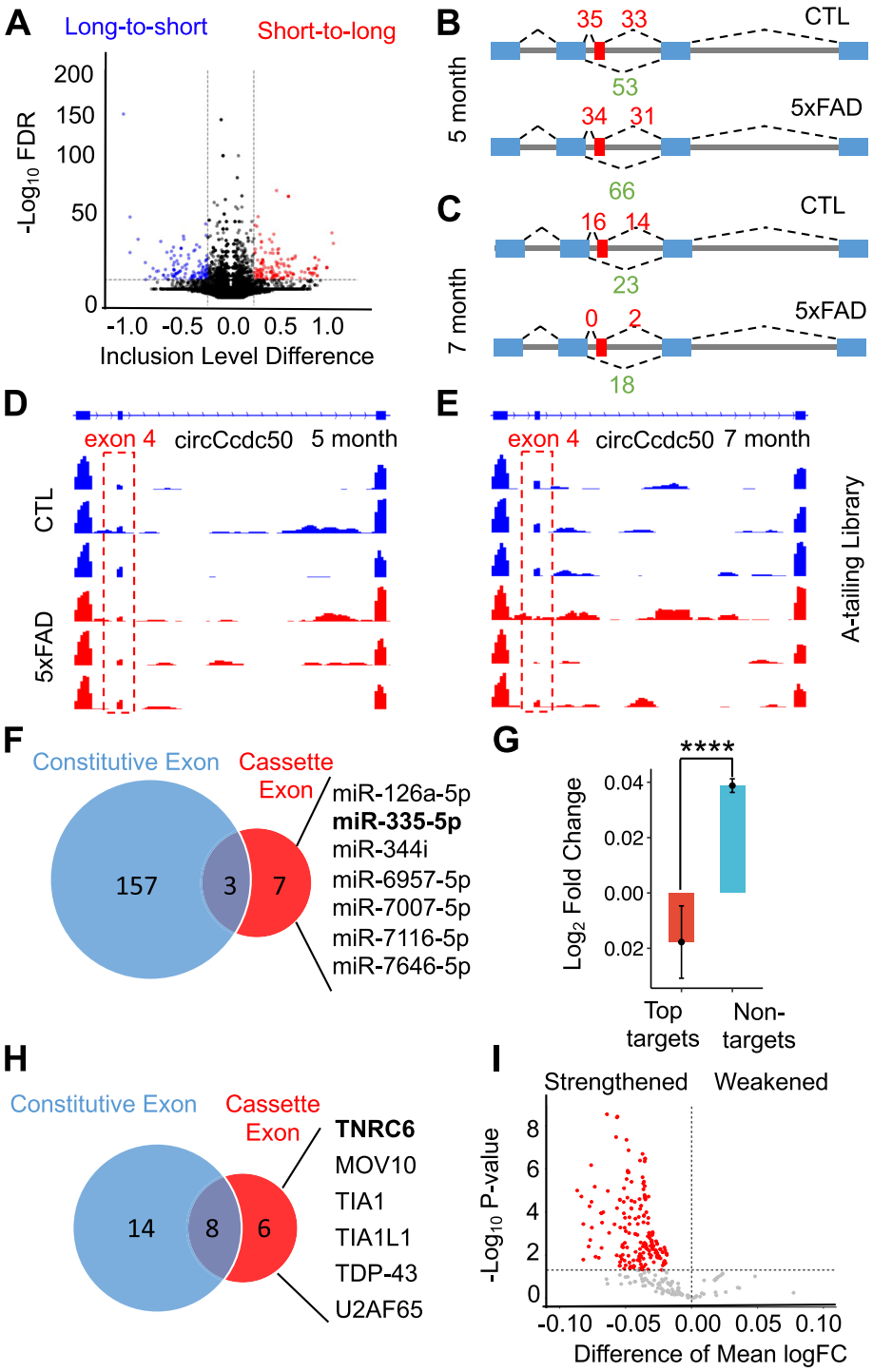

Fig. 4 (See legend on previous page.)

sequence within murine and human circGigyf2/circGIGYF2 are highly conserved (Fig. 5E). We next questioned whether circGIGYF2 (hsa_circ_0003341) is also dysregulated in AD patient brains. We mined the recently published circRNA datasets from the Mount Sinai Brain Bank (MSBB) cohort studies derived from multiple subcortical areas including BM10, BM22, BM36, and BM44 [24]. Significant downregulation of circGIGYF2 was indeed found in BM10, BM36, and BM44 using two independent algorisms (Additional file 4: Fig. S5C).

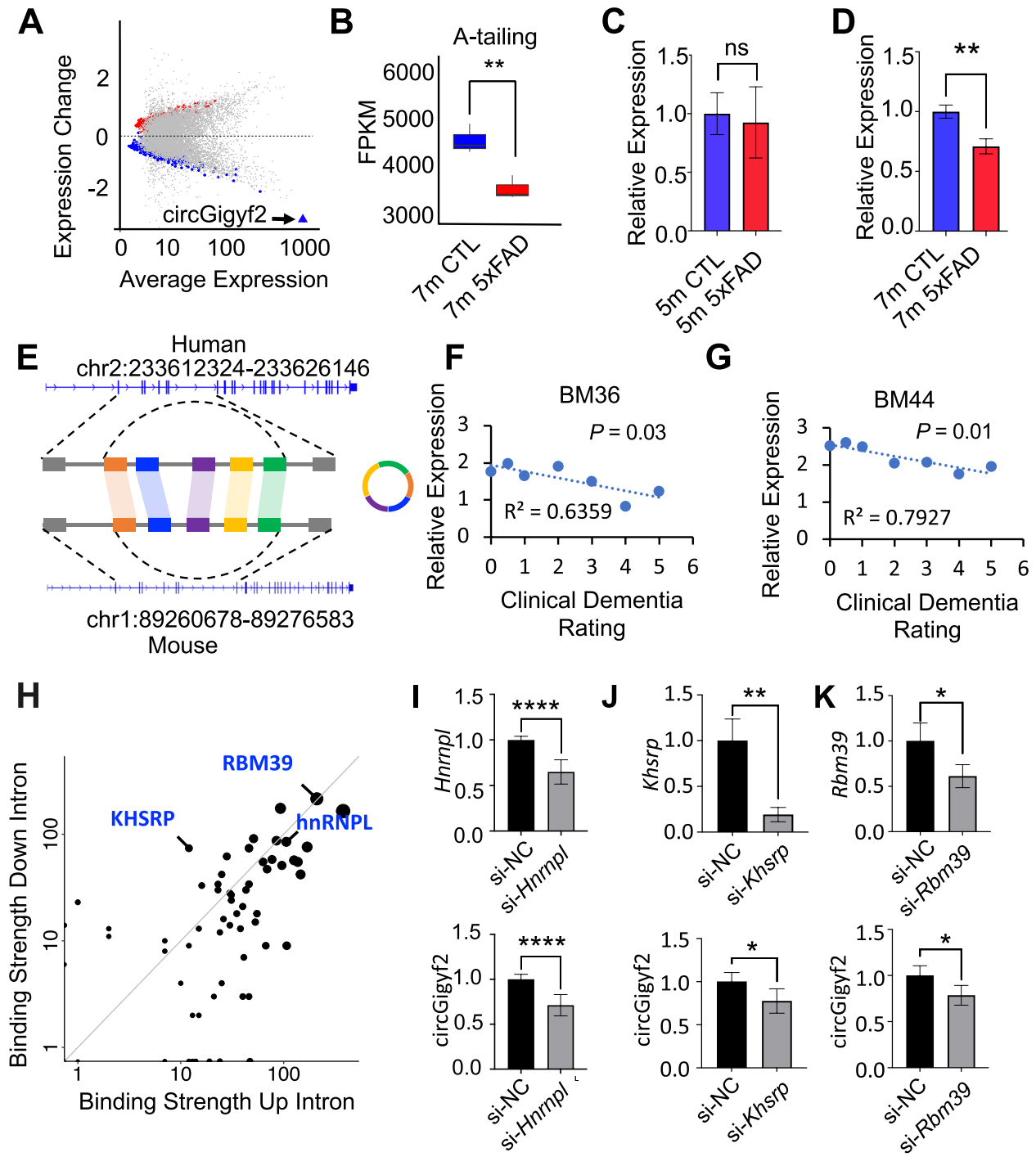

Fig. 5 CircGigyf2 is conserved and consistently downregulated in 5xFAD cortex and AD patient subcortical areas, correlated with the severity of cognitive decline, and modulated by AD-associated RBPs. **A** CircRNA expression changes identified by A-tailing/CARP in 7-month 5xFAD compared to CTL mice (FDR < 0.05). The blue triangle marks circGigyf2. **B** CircGigyf2 is significantly downregulated in A-tailing libraries of 7-month 5xFAD (red) compared to CTL (blue). **C**–**D** RT-qPCR detected no alterations of CircGigyf2 in 5-month 5xFAD cortex (**C**) but significant downregulation of CircGigyf2 in 7 months (**D**) (**$P < 0.01$, *t*-test). **E** CircGigyf2 contains five exons that are highly conserved between human (hg19) and mouse (mm9) genomic assemblies. **F**–**G** Significant reverse correlation of circGigyf2 levels in BM36 (**F**) and BM44 (**G**) with AD severity defined by the Clinical Dementia Rating in the Mount Sinai Brain Bank (MSBB) dataset (Spearman correlation). **H** Binding strength based on the numbers of predicted RBP binding sites in the flanking intron of circGigyf2 predicted by the machine-learning-based algorithm CRIP. Candidate RBP regulators are highlighted and labeled. **I** Downregulation of *Hnrnpl* mRNA (top) and circGigyf2 (bottom) upon *Hnrnpl* knockdown in N2a cells. **J** Downregulation of *Khsrp* mRNA (top) and circGigyf2 (bottom) upon *Khsrp* knockdown in N2a cells. **K** Downregulation of *Rbm39* mRNA (top) and circGigyf2 (bottom) upon *Rbm39* knockdown in N2a cells. (*$P < 0.05$, **$P < 0.01$, ****$P < 0.0001$, *t*-test)

In contrast, no reduction of circGIGYF2 was found in BM22, suggesting that circGIGYF2 is downregulated in specific subcortical areas of AD patients. Consistent with the brain region-specific AD-associated circRNA landscape (Additional file 4: Fig. S2B, C), we did not find significant alteration of circGIGYF2 in human AD entorhinal cortex [77]. Importantly, expression levels of circGIGYF2 are negatively correlated with the clinical dementia rating in BM36 ($P=0.03$) and BM44 ($P=0.01$), which indicates the severity of AD cognitive deterioration (Fig. 5F, G). These observations clearly indicated that deficiency of circGigyf2/circGIGYF2 in the cerebral cortex is associated with AD pathological progression in both the 5xFAD mouse model and AD patients, relevant to the cortical dementia phenotypes of AD.

We next set out to explore molecular mechanisms that regulate circGigyf2 biogenesis. The introns flanking the two BSJ sites of a given circRNA need to pair with each other to bring the BSJs into proximity, which in turn facilitates circRNA biogenesis [16, 17, 19]. Binding of specific RBPs to the flanking intronic sequences often bring BSJs together via protein–protein interactions, which is critical for circRNA production [16, 17, 78]. To identify RBPs that may regulate circGigyf2 biogenesis, we used a convolutional neural network-based machine learning approach, CRIP (CircRNAs interact with proteins) [42, 44], to predict nuclear RBPs binding to the introns flanking the BSJs of circGigyf2 [44]. Many nuclear RBPs were identified that exhibit high probability to bind both upstream and downstream introns flanking the BSJs of circGigyf2 (Additional File 6: Table S6, Fig. 5H), among which the splicing factors hnRNPL, which was significantly reduced in human AD postmortem brains [79], is a top hit. Multiple strong sites for potential binding to hnRNPL were found in the upstream and downstream flanking introns of circGigyf2 BSJs (Additional file 4: Fig. S5D) [80]. A closer examination identified several consensus CA motifs known for hnRNPL binding [81, 82] (Additional file 4: Fig. S5E). In addition, KHSRP and RBM39 (Fig. 5H) are also top-ranked and known to play important functions in the brain [83, 84]. To experimentally validate whether these RBPs regulate circGigyf2 biogenesis, siRNAs targeting each of these RBPs were transfected into the Neuro 2A (N2a) mouse neuroblastoma cell line. Depletion of *Hnrnpl*, *Khsrp*, or *Rbm39* individually caused a significant reduction of circGigyf2 (Fig. 5I-K), suggesting that these RBPs collectively govern circGigyf2 biogenesis.

Identification of pathologic alterations of conserved circGigyf2-miRNA pathways during AD progression

We next explored the roles of circGigyf2 in the sequestration of miRNAs, a well-defined circRNA function [16, 17]. Among the 209 putative miRNA-binding sites in mouse circGigyf2 predicted by TargetScan, 22 were also predicted in human circGIGYF2. Interestingly, miR-17-5p and miR-93-5p were predicted to bind to both mouse circGigyf2 and human circGIGYF2 with the highest probability (Fig. 6A and Additional File 7: Table S7). Downregulation of circGigyf2/circGIGYF2 in the AD brain is expected to set free its sponged miRNAs and enhance their silencing activity on target mRNAs. Indeed, significant cumulative downregulation of top mRNA targets of miR-17-5p and miR-93-5p was detected in 7-month 5xFAD cortex (Fig. 6B), while no significant changes were found at 5 months of age (Additional file 4: Fig. S6). Importantly, hyperactivity of miR-17-5p and miR-93-5p was also found in human AD patients' BM36 and BM44 subcortical areas (Fig. 6C, D). These data suggest that the circGigyf2-miR-17-5p/93-5p axis is consistently dysregulated in both 5xFAD mouse cortex and disease-relevant human AD subcortical areas. Furthermore, GO analyses from the downregulated miR-17-5p/93-5p mRNA targets revealed a significant enrichment in AD-pathology related terms, such as "regulation of neuron death" and "memory", in both 7-month 5xFAD mice cortex and human AD subcortical BM44 area (Fig. 6E, F).

To validate the predicted circGigyf2-miR-17-5p/93-5p interaction, we designed a biotinylated DNA probe specifically targeting the BSJ to pull-down circGigyf2 in the lysates derived from 7-month mouse cortex (Fig. 6G). Using divergent primers flanking the BSJ of circGigyf2, which do not amplify linear *Gigyf2* by qPCR, we detected over 50-fold enrichment of circGigyf2 in the pull-down samples from 7-month cortical lysates (Fig. 6H). Other abundant circRNAs, such as circHipk3, circPcmtd1, and circRims2, were not enriched, demonstrating the specificity of circGigyf2 pull-down. Importantly, miR-17-5p and miR-93-5p, which are predicted to strongly bind circGigyf2 (Fig. 6A and Additional File 7: Table S7), were co-isolated with circGigyf2 (Fig. 6I). In contrast, miR-671-3p, which is not predicted to bind to circGigyf2, was negligible in the circGigyf2 pull-down. Taken together, our data revealed a functional circGigyf2-miR-17-5p/93-5p pathway that is conserved in mouse and human and involved in AD pathogenesis.

Deficiency of circGigyf2 leads to altered action of sponged RBPs and downstream mRNAs associated with AD progression

Besides sponging miRNAs, circRNAs can also sequester RBPs to modulate their availability and cellular function [17]. We set out to identify RBPs that may interact with thus sponged by circGigyf2 using the machine-learning approach CRIP based on cross-linking and

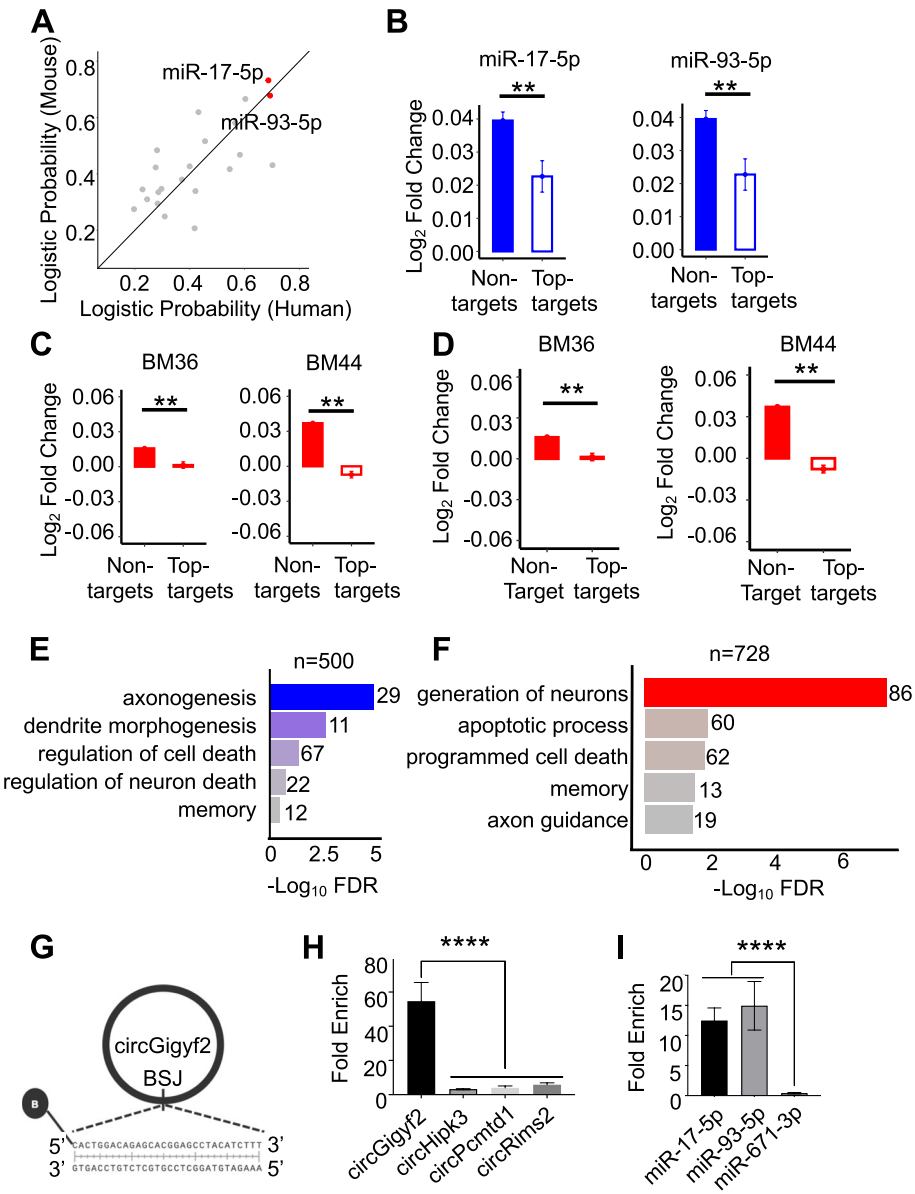

Fig. 6 CircGigyf2 downregulation leads to aberrant hyperactivity of AD-related miRNAs to suppress mRNAs involved in AD-related neuronal function. **A** Logistic binding probability of conserved miRNAs on circGigyf2 full-length sequence in human and mouse. miR17-5p and miR-93-5p (highlighted in red) show the highest binding probability. **B** Significant cumulative reduction of the top 10% confident target mRNAs (top targets) predicted by TargetScan for miR-17-5p and miR-93-5p compared with non-target mRNAs (*t*-test, $^{**}P < 0.01$). **C**–**D** Significant cumulative reduction of the top 10% confident target mRNAs (top targets) for miR-17-5p (**C**) and miR-93-5p (**D**) compared with non-target mRNAs in human postmortem subcortical areas BM36 and BM44 (*t*-test, $^{**}P < 0.01$). **E**–**F** GO analysis of downregulated genes targeted by miR-17-5p/93-5p in 7-month 5xFAD cortex (**E**) and human BM44 subcortical area (**F**). Gene number in each GO term is indicated. **G** Biotinylated DNA probe spanning circGigyf2 back splicing junction (BSJ) site were used for circGigyf2 pull-down experiment. **H** CircGigyf2 is highly enriched in circGigyf2 pull-down samples with statistical significance of fold enrichment as compared to circHipk3, circPcmtd1, and circRims2 ($^{****}P < 0.0001$, *t*-test). **I** miR-17-5p and miR-93-5p are significantly enriched in circGigyf2 pull-down samples compared to miR-671-3p, a randomly selected miRNA that is not predicted to bind circGigyf2 ($^{****}P < 0.0001$, *t*-test)

immunoprecipitation (CLIP) and sequencing datasets [44]. We calculated circGigyf2-RBP-AD risk score for each RBP based on their binding probability to circGigyf2 and their association to AD and identified multiple AD-associated RBPs that potentially interact with circGigyf2 (Fig. 7A). The cleavage and polyadenylation specific factor 6 (CPSF6), a 3′RNA processing factor critical for cleavage at the polyadenylation site (PAS)

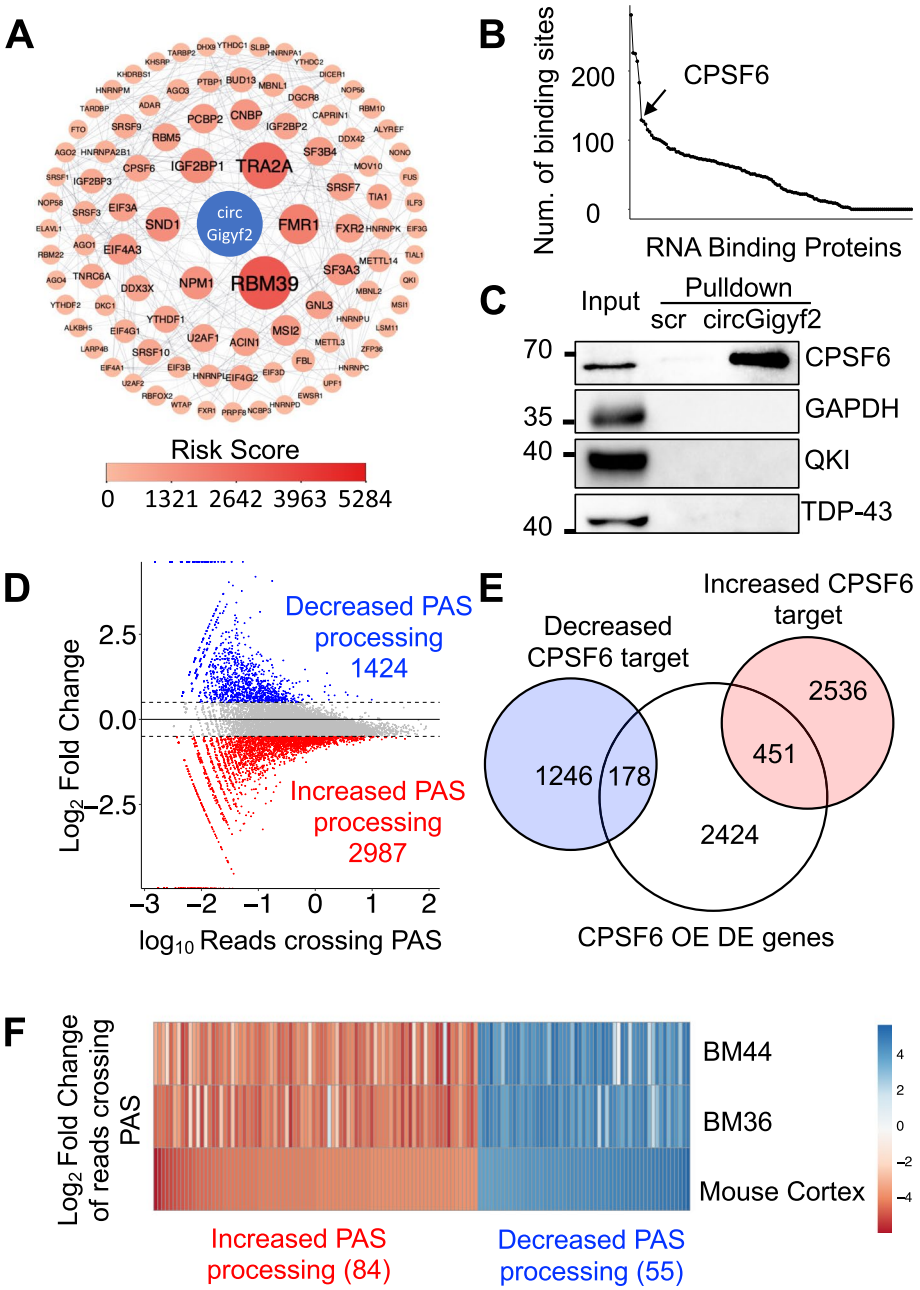

Fig. 7 AD-associated RBPs and downstream targets were affected by circGigyf2 downregulation in the 5xFAD cortex upon rapid disease progression and in AD patients' subcortical areas. **A** CircGigyf2-RBP-AD interactome. Node size and color indicating scores calculated by binding strength to circGigyf2 and AD risk for each RBP, respectively. **B** Number of binding sites for 137 RBPs in circGigyf2 full-length sequence. CPSF6 is a top hit indicated by an arrow. **C** CPSF6 is highly enriched in the pull-down sample by a circGigyf2-specific probe, while QKI, TDP-43, and GAPDH are undetectable. **D** Scatter plot of mRNAs that display altered processing efficiency at the proximal polyadenylation site (PAS) in the 7-month 5xFAD cortex. Log_{10} average and log_2 fold change of reads spanning the most proximal PAS for each gene are plotted. $|Log_2$ fold change$|>0.5$ is used as a cutoff for increased and decreased processing efficiency of proximal PAS. Increased PAS processing efficiency is indicated by less reads spanning PAS (log_2 fold change <0) and vice versa. **E** Venn diagram of genes displaying altered processing efficiency of proximal PAS in 7-month 5xFAD cortex overlapping with published RNA targets due to CPSF6 overexpression (OE) (GSE179630). The CPSF6 OE targets significantly overlap with genes with increased proximal PAS processing efficiency (Fisher exact test, $P=6.60\times10^{-6}$) but do not significantly overlap with CPSF6 targets that display decreased proximal PAS processing efficiency (Fisher exact test, $P=0.54$). **F** Heatmap shows that significantly dysregulated targets by CPSF6 OE display consistently altered (red, increased and blue, decreased) proximal PAS processing efficiency in 5xFAD mouse cortex, AD human postmortem subcortical areas BM36 and BM44

and mRNA 3′end formation that was found increased in AD patient postmortem brains [85], is top ranked for high-confident circGigyf2 binding based on the number of predicted binding sites (Fig. 7B). To experimentally validate circGigyf2-CPSF6 interaction, we performed circGigyf2 pull-down as illustrated in Fig. 6G. A robust and specific enrichment of CPSF6 was found in circGigyf2 pull-down (Fig. 7C). In contrast, Quaking (QKI) and TAR DNA-binding protein 43 (TDP-43), two RBPs that are predicted to have negligible association with circGigyf2 body, were not detected in circGigyf2 pull-down (Fig. 7C). The non-RBP glyceraldehyde-3-phosphate dehydrogenase (GAPDH) was also undetected (Fig. 7C). These data demonstrated specific interactions between circGigyf2 and CPSF6.

The downregulation of circGigyf2 in 7-month 5xFAD cortex is predicted to free up bound CPSF6.

Given the function of CPSF6 in promoting RNA cleavage at the PAS and consequent polyadenylation [48, 86], we analyzed proximal PAS processing efficiency in linear RNAs in the 5xFAD cortex using our rRNA-depleted RNA-seq dataset without A-tailing RNase R treatment (Fig. 7D) [50]. Increased PAS processing efficiency is indicated by less reads spanning the PAS and vice versa (Fig. 7D). We observed 2987 genes showing increased processing efficiency at the proximal PAS whereas 1424 genes decreased proximal PAS processing efficiency in the 7-month 5xFAD (Fig. 7D) in which downregulation of circGigyf2 is expected to release CPSF6. Moreover, genes exhibiting increased proximal PAS processing in the 7-month 5xFAD cortex significantly overlapped with genes regulated by CPSF6 over expression in HEK293T cell (GSE179630, Binomial exact test, $P=6.60\times10^{-6}$) (Fig. 7E) [48]. These data further support the conclusion that the downregulation of circGigyf2 in the 7-month 5xFAD cortex releases CPSF6, which promotes PAS processing efficiency of its targets [48, 86].

Moreover, enhanced proximal PAS processing efficiency of CPSF6 targets is also observed in the BM36 and BM44 cortical areas of AD patient postmortem brains (Fig. 7F), where circGIGYF2 expression level is negatively associated with dementia severity (Fig. 5F, G). Genes with enhanced proximal PAS processing in both 5xFAD mouse cortex and AD patient subcortical areas were significantly enriched in Gene Ontology (GO) processes relevant to AD phenotype, such as "learning" and "neuron apoptotic process" (Additional file 4: Fig. S7A). Moreover, circGIGYF2-CPSF6 targets are enriched in multiple KEGG pathways related to neurodegeneration disorders (Additional file 4: Fig. S7B). Together, these data provide a strong example that AD progression-associated dysregulation of a circRNA can lead to pathological changes of conserved circRNA-RBP-mRNA network in AD.

circGigyf2 deficiency causes dysregulation of miR93-5p/17-5p and CPSF6 targets, leading to increased neuronal apoptosis upon insult

To definitively address whether circGigyf2 plays causative roles in regulating the miR-93-5p/17-5p-mRNA pathway and the CPSF6-mRNA pathway in neurons, we performed siRNA knockdown (KD) of circGigyf2 in an immortalized mouse neuronal cell line Cath.-a-differentiated (CAD). RT-qPCR using divergent primers specifically targeting circGigyf2 confirmed 45% of circGigyf2 knockdown in CAD cells (Fig. 8A). Indeed, genes displaying increased proximal PAS processing efficiency caused by circGigyf2 KD significantly overlap with those in 5xFAD mouse cortex (Binomial exact test, $P=2.19\times10^{-8}$), with 551 in common (Fig. 8B). Among these genes, we focused on CPSF6 OE targets and examined their proximal PAS processing changes in human AD patients' BM36 and BM44 areas [48]. We found that fifty (50) CPSF6 targets showed commonly enhanced proximal PAS processing in 7-month 5xFAD mouse cortex, human AD BM36, and BM44 subcortical areas, as well as circGigyf2 KD CAD cells (Fig. 8C). Consistent with the identified GO terms (Additional file 4: Fig. S7A), we found commonly regulated CPSF6 genes including *Fam162a*, *Prdx2*, and *Aldh1a3*, which are known to be involved in neuronal apoptotic process (Fig. 8C).

Moreover, circGigyf2 KD in CAD cell caused downregulation of 410 miR-17-5p/93-5p targets, which significantly overlap with miR-17-5p/93-5p targets affected in the 7-month 5xFAD cortex (Binomial exact test, $P=0.019$), with 200 targets in common (Fig. 8D). Of note, among these miR-17-5p/93-5p targets downregulated by circGigyf2 KD, we identified multiple apoptotic inhibitor genes, represented by *Ccnd2*, *Bcl11b*, *Oxr1*, and *Alg3* that are commonly reduced in 7-month 5xFAD cortex, BM36/BM44 AD patient subcortical areas and circGigyf2 KD CAD cells (Fig. 8E).

To directly test whether circGigyf2 deficiency can indeed potentiate neuron apoptosis, we challenged circGigyf2 KD CAD cells with C2-ceramide that is known to induce apoptosis and quantified apoptotic cells by TUNEL assay. The number of apoptotic cells is significantly increased in circGigyf2 KD CAD cells as compared to control siRNA-treated cells (Fig. 8F, G). These results clearly demonstrated causative roles of circGigyf2 deficiency in neuronal death, which is highly relevant to the loss of brain neurons in AD mouse models and neuronal degeneration in AD patients [87, 88]. To our knowledge, this is the first example in which neuronal death is caused by an AD-affected circRNA through integrating abnormalities in downstream miRNA-mRNA and RBP-mRNA pathways.

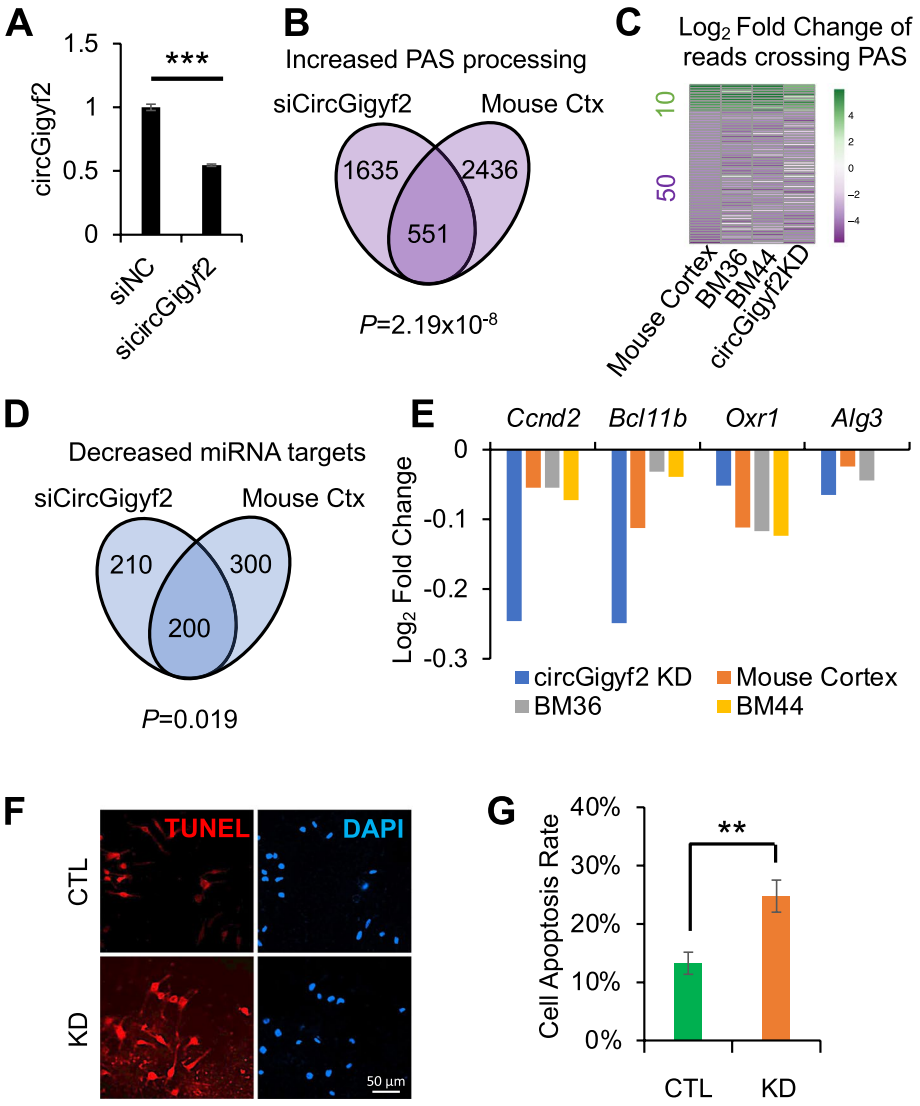

Fig. 8 Knockdown of circGigyf2 enhances miR-17-5p/93-5p activity, CPSF6-mediated proximal PAS processing, and neuronal responses to apoptotic insults. **A** Efficient knockdown of circGigyf2 by siRNA in mouse central nervous system (CNS) catecholaminergic cell line Cath.-a-differentiated (CAD) cell (*** represents $P < 0.001$, *t*-test). **B** Overlap of genes with increased proximal PAS processing efficiency in 7-month 5xFAD cortex and circGigyf2 KD in CAD cell. **C** Heatmap shows altered proximal PAS processing efficiency as a consequence of circGigyf2 KD in CAD cells, recapitulating those commonly found in 5xFAD cortex and human AD postmortem cortex. **D** Overlap of downregulated miR-17-5p/93-5p targets in 7-month 5xFAD cortex and circGigyf2 KD in CAD cell. **E** Downregulation of multiple miR-17-5p/93-5p targeted apoptotic suppressors in 7-month 5xFAD mouse cortex, human AD BM36 and BM44 and circGigyf2 KD in CAD cell. **F** Representative images of apoptotic CAD cells induced by C2-ceremide in circGigyf2 KD and control group based on the TUNEL assay. **G** Percentage of cell apoptosis induced by C2-ceremide calculated by number of apoptosis cells (TUNEL)/number of all cells (DAPI)

Discussion

Despite the growing body of evidence documenting circRNA abnormalities in multiple brain regions of AD patients [14, 24, 30, 77], whether and how circRNA dysregulation contributes to early pathogenesis and/or progression of AD cannot be addressed by human postmortem studies that represent an end-stage snapshot of the disease. Whether the disrupted circRNA landscape plays causative roles in AD pathogenesis or is an ultimate result of massive neurodegeneration is a prevailing obstacle in postmortem studies. Alternative strategies are needed to uncover the molecular mechanisms that cause dysregulation of circRNA biogenesis, which in turn affects downstream gene networks that contribute to AD pathogenesis. In this regard, AD mouse models, although may only mimic specific aspects of AD pathology, allow

the identification of circRNAs associated with AD progression. These circRNAs are conserved and affected in AD patient brains as well, which may serve as pathological biomarkers to monitor the disease progression. Moreover, the biochemical interactions between AD progression-associated circRNAs and their sponged miRNAs and RBPs in fresh AD mouse brain tissues can be experimentally validated to identify direct molecular mechanisms and biological pathways that may contribute to AD pathogenesis.

The cerebral cortex of AD patients harbors profound hallmark pathology that underlies the clinical manifestation of cortical dementia [36]. Our studies identified circRNA landscape alterations in the 5xFAD mouse cortex that are specifically associated with the fast progression of AD pathological phenotypes. Although 7 months of age denotes the fully onset of AD phenotypes to a therapeutically irreversible stage in 5xFAD mice, these mice still do not reach to the end point of the disease states. Nonetheless, hundreds of such dysregulated circRNAs are shared in postmortem subcortical areas of AD patients, suggesting their key pathogenic roles. These observations provide the first evidence that broad circRNA dysregulation occurs long before and may persist toward the end stage of the disease. Moreover, we discovered dysregulation of novel circRNA clusters and circRNA splice variants that cooperate with multiple affected individual circRNAs to form a pathogenic circRNA hub, which collectively affects downstream pathways in AD progression. Although dysregulation of specific circRNAs of low abundance or individual circRNAs within a cluster often does not reach statistical significance, our data suggests they can function together as a group to exert additive impacts on downstream targets. These previously underappreciated events added additional layers and functional importance of circRNA dysregulation. Unfortunately, circRNA-clusters and cassette exon switch could not be analyzed in the majority of publicly available AD patients' RNA-seq datasets due to the lack of A-tailing RNase R treatment in those studies thus inability for precise annotation of the full-length circRNA sequence [38].

Surprisingly, distinct circRNAs are dysregulated in different AD brain regions, regardless of the relatively similar expression landscape. This is clearly shown when comparing the AD-affected circRNA landscapes in the 5xFAD cortex and hippocampus, although both brain regions are comparably affected by AD pathology at 7 months of age [54]. Brain-region-specific dysregulation of circRNAs is also observed in postmortem subcortical areas of AD patients. In fact, only five circRNAs were found consistently dysregulated in both the entorhinal and parietal cortex [77]. In addition, the AD entorhinal cortex showed much less commonly dysregulated circRNAs found in the 5xFAD cortex as compared to other cortical areas of AD patients. These interesting observations from systematic comparisons suggest that dysregulation of distinct circRNAs, hence their downstream pathways, may contribute to brain-region-specific pathogenesis and clinical phenotypes at different stages of AD progression.

Discovering circRNAs dysregulated during AD progression in murine models not only allowed us to identify conserved circRNAs that are also affected in AD patient brains but also revealed the early progressive changes of such dysregulation along disease development. One example is circGigyf2, which is specifically downregulated in 5xFAD cerebral cortex with the highest net change upon the development of the full spectrum of AD pathological phenotypes at 7 months of age. Importantly, in the AD patients postmortem brain datasets, we found that the progressive decline of circGIGYF2 in multiple subcortical areas is significantly associated with the severity of intellectual deterioration in AD patients, including inferior frontal gyrus (BM44) and parahippocampal gyrus (BM36), two most vulnerable subcortical areas in AD that are important in language processing, memory encoding, and retrieval [63]. In agreement with region-specific circRNA dysregulation in AD, circGIGYF2 is not significantly altered in either AD patients' hippocampus [30] or entorhinal cortex [77]. Thus, we demonstrated that the profile of circRNA dysregulation represented by circGIGYF2 is associated with AD pathologic advancement in a brain-region-specific manner, which could serve as a biomarker indicative of AD progression.

We also established strategies using advanced computational analysis to identify the upstream and downstream molecular factors centered on circGigyf2, many of which are affected in AD thus forming a pathological pathway. By combining in silico computational prediction and experimental validation, we identified multiple RBPs necessary for the efficient biogenesis of circGigyf2, including hnRNPL, RBM39, and KHSRP. Of note, expression of hnRNPL is reduced in neurons with granulovacuolar degeneration, which is a common feature in AD [79]. Dysfunction of the RBM39 ortholog in *Drosophila* not only affects neurogenesis but also results in aberrant behavioral phenotypes [89]. In addition, KHSRP loss of function leads to impaired prefrontal-dependent memory consolidation [84]. These RBPs are highly conserved, hence suggesting common upstream regulators in the biogenesis of AD-associated circRNAs.

The high abundance of circGigyf2 offers feasibility for efficient sponging of miRNAs and RBPs [84]. In searching for AD-associated downstream pathways, we discovered conserved malfunction of miRNA and RBP pathways

caused by circGigyf2 deficiency in both the 5xFAD cortex and AD patients' postmortem brains, represented by the circGigyf2-sponged miR-17-5p/93-5p and CPSF6. Consistent with the hyperactivity of miR-17-5p/93-5p pathway associated with the reduction of circGigyf2 in the 5xFAD cortex, increased activity of miR-17-5p/93-5p is widely reported in AD patients [84, 90], which uncovered a conserved pathological circRNA-miRNA pathway in AD pathogenesis. Compared to the well-established roles of circRNA in modulating miRNA activities, identification of the circRNA-RBP-mRNA axis is a much more challenging task and unfortunately understudied. Using advanced deep learning strategies, we identified putative binding sites for multiple RBPs in circGigyf2. Among the top hits, CPSF6 that governs cleavage and processing at the PAS for the 3′ end formation of mRNAs, has been shown to be associated with AD pathology [85]. Reduction of circGigyf2 is predicted to release sponged CPSF6, hence alter PAS processing efficiency of many transcripts. Consistent with this idea, we identified an aberrant increase of numerous previously reported human CPSF6 mRNA targets in both the 5xFAD cortex and human AD postmortem brains. Importantly, knockdown circGigyf2 in an immortalized mouse neuronal cell line in culture vastly recapitulated dysregulation of miR-17-5p/93-5p and CPSF6 targets in both the 5xFAD mouse cortex and human AD patients' subcortical areas. These results clearly demonstrated the causal roles of circGigyf2 deficiency in dysregulation of the conserved miRNA-mRNA and RBP-mRNA axes.

Interestingly, dysregulated miR-17-5p/93-5p or CPSF6 mRNA targets caused by circGigyf2 deficiency that are shared in mouse and human are enriched in the apoptotic pathway. Indeed, circGigyf2 knockdown significantly increased neuronal death responses upon apoptotic insult, which strongly support the pathological significance of circGigyf2 deficiency relevant to the neuronal loss. Taken together, these data identified a conserved network composed by converged RBP-mRNA and miRNA-mRNA pathways affected by circGigyf2 deficiency that underlie neuronal apoptosis in the progression of AD pathogenesis, which is highly translatable from an AD mouse model to human AD patients.

In addition to sponging miRNAs and RBPs, emerging evidence suggests multifaceted mechanisms of circRNA action in controlling brain function. In fact, many circRNAs harbor short open reading frames (ORFs) immediately downstream of ribosome internal entry site (IRES)-like sequence motifs and thus may be translated and produce small peptides in the cytoplasm [91–93]. Noticeably, mouse and human circGigyf2 does contain an ORF in frame with the ORF in its linear host mRNA that encodes GIGYF2. At this point, whether the circGigyf2 ORF is indeed translated in neurons and produces a truncated peptide thus contributing to AD phenotypes remains elusive and will be the next challenge for future studies. Recent publication also demonstrated A-to-I editing could potentially promote circRNA translation [77], which will also be an interesting point for future study.

Conclusions

Our study demonstrated brain-region-specific disruption of the circRNA landscape in an AD mouse model during early pathological progression and identified conserved signature circRNAs that are also affected in AD patients at the end stage, which could hold promise as potential biomarkers for monitoring irreversible pathological progression and disease acceleration. We also demonstrated causative roles and molecular mechanisms of AD-affected circRNAs that lead to the malfunction of downstream gene networks shared in mouse and human that underlie AD pathogenesis. These findings comprehensively improved the current mechanistic understanding of how circRNA abnormalities contribute to AD pathogenesis and progression. Moreover, our studies established a strategy of using mouse models to complement patients' postmortem studies, which leads to the identification of conserved pathological networks that underlie the long progression of aging-dependent disorders.

Supplementary Information

The online version contains supplementary material available at https://doi.org/10.1186/s13073-024-01404-6.

Additional File 1: Table S1. List of qPCR Primers to detect the expression levels of circRNAs, genes and miRNAs used in this study.

Additional File 2: Table S2. Reagents and resources used in this study.

Additional File 3: Table S3. Published AD phenotype and treatment in 5-month and 7-month of AD mouse model. Published AD phenotype and treatment in 5-month and 7-month 5xFAD mice. Behavioral, physiological, and pathological AD phenotypes in 5-month and 7-month-old 5xFAD mice. Treatments that prevent AD early progression phenotypes were also listed.

Additional File 4: Supplementary Figures S1-S7.

Additional File 5: Table S4. Differential expression analysis of circRNAs in 5-month and 7-month 5xFAD and their age-matched littermates. Average normalized circRNA expression levels of control and AD mice at both 5-month and 7-month of ages were shown. Log fold changes (LogFC) and their overall ranking based on LogFC were indicated. Table S5: The expression analysis of 7-month AD-associated circRNA host genes. The normalized expression level of each replicate, LogFC and FDR were indicated.

Additional File 6: Table S6. Nuclear RBP binding sites in 1000 nucleotides (nt) sequence of upstream and downstream intron of mouse circGigyf2 predicted by CRIP (CircRNAs Interact with Proteins). The number of putative binding sites of each RNA-binding proteins (RBPs) upstream and downstream of circGigyf2 flanking introns were indicated.

Additional File 7: Table S7. Binding probability of common miRNAs that are sponged by both mouse circGigyf2 and human circGIGYF2. miR-17-5p and miR-93-5p are highlighted in red based on their significant activity change ($P < 0.05$) and high binding probability.

Acknowledgements
We thank all members from Yao lab and Feng Lab for their support and suggestions in the project.

Authors' contributions
F.W., Y.L., Y.F. and B.Y. conceived and designed the study. F.W. performed most of the experiments. H. S. and P.T. assisted with the experiments. F.W. and H.S. prepared mouse colonies and collected brain tissues. Y.L., F.W., S.K. and B.Y. performed bioinformatics analysis. L.C. authorized access to MSBB dataset from AMP-AD Knowledge Portal. J. H. and L.C. assisted the statistical analysis. F.W., Y.L., Y.F. and B.Y. wrote the manuscript with input from all the other authors. P.M.-F. and X.J. assisted with the experiments and edited the manuscript. All authors have read and approved the final manuscript.

Funding
This work was supported by the following funding sources: NIH grants R01MH117122, R01AG062577, R01AG064786, R33NS106120, and R01AG078937 to B.Y, R01NS118819 to Y.F. and B.Y, and R01NS110110 to YF.

Data availability
The dataset supporting the conclusions of this article is available in the GEO repository under accession numbers GSE236683 [94], GSE272744 [95], and GSE272745 [96]. RNA-seq data for multiple human postmortem subcortical areas including the frontal pole (BM10, $n=317$), superior temporal gyrus (BM22, $n=324$), parahippocampal gyrus (BM36, $n=311$), and inferior frontal gyrus (BM44, $n=301$) generated from Mount Sinai Brain Bank (MSBB) cohort were downloaded from Synapse database (https://www.synapse.org/Synapse:syn7416949) [31]. RNA-seq data for CPSF6 overexpression was downloaded from Gene Expression Omnibus (GSE179630) [48] to identify CPSF6 targets. Raw image of the Western blot is published in Mendeley Data. (https://data.mendeley.com/datasets/vmz7m7t9zb/1). All original code has been deposited at Code availability Homemade R script used in this study is publicly available on GitHub (https://github.com/YaoLabEmory/ADcircRNA) [97]. Any additional information required to reanalyze the data reported in this paper is available from the lead contact upon request.

Declarations

Ethics approval and consent to participate
All animal procedures and protocols were approved by the Emory University Institutional Animal Care and Use Committee (protocol ID: PROTO201800040). This manuscript does not include any work performed with human participants.

Consent for publication
Not applicable.

Competing interests
The authors declare no competing interests.

Author details
[1]Department of Human Genetics, Emory University School of Medicine, Atlanta, GA 30322, USA. [2]Department of Pharmacology and Chemical Biology, Emory University School of Medicine, Atlanta, GA 30322, USA. [3]Department of Biostatistics, College of Public Health and Health Professions & College of Medicine, University of Florida, Gainesville, FL 32611, USA.

Received: 28 July 2024 Accepted: 30 October 2024
Published online: 11 November 2024

References

1. Kabacik S, Lowe D, Fransen L, Leonard M, Ang SL, Whiteman C, Corsi S, Cohen H, Felton S, Bali R, et al. The relationship between epigenetic age and the hallmarks of aging in human cells. Nat Aging. 2022;2:484–93.
2. Whitehouse PJ. The concept of subcortical and cortical dementia: another look. Ann Neurol. 1986;19:1–6.
3. Mouton PR, Martin LJ, Calhoun ME, Dal Forno G, Price DL. Cognitive decline strongly correlates with cortical atrophy in Alzheimer's dementia. Neurobiol Aging. 1998;19:371–7.
4. Farlow MR. Etiology and pathogenesis of Alzheimer's disease. Am J Health Syst Pharm. 1998;55:S5–10.
5. Karch CM, Goate AM. Alzheimer's disease risk genes and mechanisms of disease pathogenesis. Biol Psychiatry. 2015;77:43–51.
6. Yoshikai S, Sasaki H, Doh-ura K, Furuya H, Sakaki Y. Genomic organization of the human amyloid beta-protein precursor gene. Gene. 1990;87:257–63.
7. O'Brien RJ, Wong PC. Amyloid precursor protein processing and Alzheimer's disease. Annu Rev Neurosci. 2011;34:185–204.
8. Mullan M, Crawford F, Axelman K, Houlden H, Lilius L, Winblad B, Lannfelt L. A pathogenic mutation for probable Alzheimer's disease in the APP gene at the N–terminus of β–amyloid. Nat Genet. 1992;1:345–7.
9. Esteller M. Non-coding RNAs in human disease. Nat Rev Genet. 2011;12:861–74.
10. Millan MJ. Linking deregulation of non-coding RNA to the core pathophysiology of Alzheimer's disease: an integrative review. Prog Neurobiol. 2017;156:1–68.
11. Tan L, Yu JT, Hu N, Tan L. Non-coding RNAs in Alzheimer's disease. Mol Neurobiol. 2013;47:382–93.
12. Guevremont D, Tsui H, Knight R, Fowler CJ, Masters CL, Martins RN, Abraham WC, Tate WP, Cutfield NJ, Williams JM. Plasma microRNA vary in association with the progression of Alzheimer's disease. Alzheimers Dement (Amst). 2022;14:e12251.
13. Hebert SS, Horre K, Nicolai L, Papadopoulou AS, Mandemakers W, Silahtaroglu AN, Kauppinen S, Delacourte A, De Strooper B. Loss of microRNA cluster miR-29a/b-1 in sporadic Alzheimer's disease correlates with increased BACE1/beta-secretase expression. Proc Natl Acad Sci U S A. 2008;105:6415–20.
14. Dube U, Del-Aguila JL, Li Z, Budde JP, Jiang S, Hsu S, Ibanez L, Fernandez MV, Farias F, Norton J, et al. An atlas of cortical circular RNA expression in Alzheimer disease brains demonstrates clinical and pathological associations. Nat Neurosci. 2019;22:1903–12.
15. Akhter R. Circular RNA and Alzheimer's Disease. Adv Exp Med Biol. 2018;1087:239–43.
16. Kristensen LS, Andersen MS, Stagsted LVW, Ebbesen KK, Hansen TB, Kjems J. The biogenesis, biology and characterization of circular RNAs. Nat Rev Genet. 2019;20:675–91.
17. Chen LL. The expanding regulatory mechanisms and cellular functions of circular RNAs. Nat Rev Mol Cell Biol. 2020;21:475–90.
18. Yang L, Wilusz JE, Chen LL. Biogenesis and regulatory roles of circular RNAs. Annu Rev Cell Dev Biol. 2022;38:263–89.
19. Liu CX, Chen LL. Circular RNAs: Characterization, cellular roles, and applications. Cell. 2022;185:2016–34.
20. Rybak-Wolf A, Stottmeister C, Glazar P, Jens M, Pino N, Giusti S, Hanan M, Behm M, Bartok O, Ashwal-Fluss R, et al. Circular RNAs in the mammalian brain are highly abundant, conserved, and dynamically expressed. Mol Cell. 2015;58:870–85.
21. You X, Vlatkovic I, Babic A, Will T, Epstein I, Tushev G, Akbalik G, Wang M, Glock C, Quedenau C, et al. Neural circular RNAs are derived from synaptic genes and regulated by development and plasticity. Nat Neurosci. 2015;18:603–10.
22. Cai H, Li Y, Niringiyumukiza JD, Su P, Xiang W. Circular RNA involvement in aging: an emerging player with great potential. Mech Ageing Dev. 2019;178:16–24.
23. Doxakis E. Insights into the multifaceted role of circular RNAs: implications for Parkinson's disease pathogenesis and diagnosis. NPJ Parkinsons Dis. 2022;8:7.
24. Lo I, Hill J, Vilhjalmsson BJ, Kjems J. Linking the association between circRNAs and Alzheimer's disease progression by multi-tissue circular RNA characterization. RNA Biol. 2020;17:1789–97.
25. Errichelli L, Dini Modigliani S, Laneve P, Colantoni A, Legnini I, Capauto D, Rosa A, De Santis R, Scarfò R, Peruzzi G, et al. FUS affects circular RNA expression in murine embryonic stem cell-derived motor neurons. Nat Commun. 2017;8:14741.
26. Conn Simon J, Pillman Katherine A, Toubia J, Conn Vanessa M, Salmanidis M, Phillips Caroline A, Roslan S, Schreiber Andreas W, Gregory Philip A, Goodall Gregory J. The RNA binding protein quaking regulates formation of circRNAs. Cell. 2015;160:1125–34.
27. Hanan M, Soreq H, Kadener S. CircRNAs in the brain. RNA Biol. 2017;14:1028–34.
28. Gruner H, Cortés-López M, Cooper DA, Bauer M, Miura P. CircRNA accumulation in the aging mouse brain. Sci Rep. 2016;6:38907.

29. Floris G, Zhang L, Follesa P, Sun T. Regulatory role of circular RNAs and neurological disorders. Mol Neurobiol. 2017;54:5156–65.
30. Puri S, Hu J, Sun Z, Lin M, Stein TD, Farrer LA, Wolozin B, Zhang X. Identification of circRNAs linked to Alzheimer's disease and related dementias. Alzheimers Dement. 2023;19:3389–405.
31. Wang M, Beckmann ND, Roussos P, Wang E, Zhou X, Wang Q, Ming C, Neff R, Ma W, Fullard JF, et al. The Mount Sinai cohort of large-scale genomic, transcriptomic and proteomic data in Alzheimer's disease. Scientific Data. 2018;5:180185.
32. Jeck WR, Sorrentino JA, Wang K, Slevin MK, Burd CE, Liu J, Marzluff WF, Sharpless NE. Circular RNAs are abundant, conserved, and associated with ALU repeats. RNA. 2013;19:141–57.
33. Oakley H, Cole SL, Logan S, Maus E, Shao P, Craft J, Guillozet-Bongaarts A, Ohno M, Disterhoft J, Van Eldik L, et al. Intraneuronal beta-amyloid aggregates, neurodegeneration, and neuron loss in transgenic mice with five familial Alzheimer's disease mutations: potential factors in amyloid plaque formation. J Neurosci. 2006;26:10129–40.
34. Richard BC, Kurdakova A, Baches S, Bayer TA, Weggen S, Wirths O. Gene dosage dependent aggravation of the neurological phenotype in the 5XFAD mouse model of Alzheimer's disease. J Alzheimers Dis. 2015;45:1223–36.
35. Sasaguri H, Nilsson P, Hashimoto S, Nagata K, Saito T, De Strooper B, Hardy J, Vassar R, Winblad B, Saido TC. APP mouse models for Alzheimer's disease preclinical studies. EMBO J. 2017;36:2473–87.
36. Forner S, Kawauchi S, Balderrama-Gutierrez G, Kramar EA, Matheos DP, Phan J, Javonillo DI, Tran KM, Hingco E, da Cunha C, et al. Systematic phenotyping and characterization of the 5xFAD mouse model of Alzheimer's disease. Sci Data. 2021;8:270.
37. Xiao MS, Wilusz JE. An improved method for circular RNA purification using RNase R that efficiently removes linear RNAs containing G-quadruplexes or structured 3′ ends. Nucleic Acids Res. 2019;47:8755–69.
38. Li Y, Wang F, Teng P, Ku L, Chen L, Feng Y, Yao B. Accurate identification of circRNA landscape and complexity reveals their pivotal roles in human oligodendroglia differentiation. Genome Biol. 2022;23:48.
39. Wang H, Dictenberg JB, Ku L, Li W, Bassell GJ, Feng Y. Dynamic association of the fragile X mental retardation protein as a messenger ribonucleoprotein between microtubules and polyribosomes. Mol Biol Cell. 2008;19:105–14.
40. Sun T, Zeng L, Cai Z, Liu Q, Li Z, Liu R. Comprehensive analysis of dysregulated circular RNAs and construction of a ceRNA network involved in the pathology of Alzheimer's disease in a 5 x FAD mouse model. Front Aging Neurosci. 2022;14:1020699.
41. Chen L, Wang F, Bruggeman EC, Li C, Yao B. circMeta: a unified computational framework for genomic feature annotation and differential expression analysis of circular RNAs. Bioinformatics. 2020;36:539–45.
42. Zhang K, Pan X, Yang Y, Shen HB. CRIP: predicting circRNA-RBP interaction sites using a codon-based encoding and hybrid deep neural networks. RNA. 2019;25(12):1604–15.
43. Pan X, Fang Y, Li X, Yang Y, Shen HB. RBPsuite: RNA-protein binding sites prediction suite based on deep learning. BMC Genomics. 2020;21:884.
44. Dammer EB, Duong DM, Diner I, Gearing M, Feng Y, Lah JJ, Levey AI, Seyfried NT. Neuron enriched nuclear proteome isolated from human brain. J Proteome Res. 2013;12:3193–206.
45. Kim D, Pertea G, Trapnell C, Pimentel H, Kelley R, Salzberg SL. TopHat2: accurate alignment of transcriptomes in the presence of insertions, deletions and gene fusions. Genome Biol. 2013;14:1–13.
46. Trapnell C, Roberts A, Goff L, Pertea G, Kim D, Kelley DR, Pimentel H, Salzberg SL, Rinn JL, Pachter L. Differential gene and transcript expression analysis of RNA-seq experiments with TopHat and Cufflinks. Nat Protoc. 2012;7:562–78.
47. Resource TGO. 20 years and still GOing strong. Nucleic Acids Res. 2019;47:D330–8.
48. Ghosh S, Ataman M, Bak M, Borsch A, Schmidt A, Buczak K, Martin G, Dimitriades B, Herrmann CJ, Kanitz A, Zavolan M. CFIm-mediated alternative polyadenylation remodels cellular signaling and miRNA biogenesis. Nucleic Acids Res. 2022;50:3096–114.
49. Agarwal V, Bell GW, Nam JW, Bartel DP. Predicting effective microRNA target sites in mammalian mRNAs. Elife. 2015;4:e05005.
50. Wang R, Zheng D, Yehia G, Tian B. A compendium of conserved cleavage and polyadenylation events in mammalian genes. Genome Res. 2018;28:1427–41.
51. Liao Y, Smyth GK, Shi W. featureCounts: an efficient general purpose program for assigning sequence reads to genomic features. Bioinformatics. 2014;30:923–30.
52. Arboleda G, Waters C, Gibson RM. Metabolic activity: a novel indicator of neuronal survival in the murine dopaminergic cell line CAD. J Mol Neurosci. 2005;27:065–78.
53. Love MI, Huber W, Anders S. Moderated estimation of fold change and dispersion for RNA-seq data with DESeq2. Genome Biol. 2014;15:550.
54. Trapnell C, Hendrickson DG, Sauvageau M, Goff L, Rinn JL, Pachter L. Differential analysis of gene regulation at transcript resolution with RNA-seq. Nat Biotechnol. 2013;31:46–53.
55. Zeng Y, Zhang J, Zhu Y, Zhang J, Shen H, Lu J, Pan X, Lin N, Dai X, Zhou M, Chen X. Tripchlorolide improves cognitive deficits by reducing amyloid beta and upregulating synapse-related proteins in a transgenic model of Alzheimer's Disease. J Neurochem. 2015;133:38–52.
56. Jeong YJ, Son Y, Park HJ, Oh SJ, Choi JY, Ko YG, Lee HJ. Therapeutic effects of aripiprazole in the 5xFAD Alzheimer's disease mouse model. Int J Mol Sci. 2021;22:9374.
57. Wang K, Singh D, Zeng Z, Coleman SJ, Huang Y, Savich GL, He X, Mieczkowski P, Grimm SA, Perou CM, et al. MapSplice: accurate mapping of RNA-seq reads for splice junction discovery. Nucleic Acids Res. 2010;38:e178.
58. Memczak S, Jens M, Elefsinioti A, Torti F, Krueger J, Rybak A, Maier L, Mackowiak SD, Gregersen LH, Munschauer M, et al. Circular RNAs are a large class of animal RNAs with regulatory potency. Nature. 2013;495:333–8.
59. Zhang J, Chen S, Yang J, Zhao F. Accurate quantification of circular RNAs identifies extensive circular isoform switching events. Nat Commun. 2020;11:90.
60. Zhang XO, Dong R, Zhang Y, Zhang JL, Luo Z, Zhang J, Chen LL, Yang L. Diverse alternative back-splicing and alternative splicing landscape of circular RNAs. Genome Res. 2016;26:1277–87.
61. Hansen TB, Veno MT, Damgaard CK, Kjems J. Comparison of circular RNA prediction tools. Nucleic Acids Res. 2016;44:e58.
62. Wu DP, Zhao YD, Yan QQ, Liu LL, Wei YS, Huang JL. Circular RNAs: emerging players in brain aging and neurodegenerative diseases. J Pathol. 2023;259:1–9.
63. Wang M, Roussos P, Mckenzie A, Zhou X, Kajiwara Y, Brennand KJ, De Luca GC, Crary JF, Casaccia P, Buxbaum JD, et al. Integrative network analysis of nineteen brain regions identifies molecular signatures and networks underlying selective regional vulnerability to Alzheimer's disease. Genome Medicine. 2016;8:104.
64. Newman AM, Steen CB, Liu CL, Gentles AJ, Chaudhuri AA, Scherer F, Khodadoust MS, Esfahani MS, Luca BA, Steiner D, et al. Determining cell type abundance and expression from bulk tissues with digital cytometry. Nat Biotechnol. 2019;37:773–82.
65. Zhang Y, Sloan SA, Clarke LE, Caneda C, Plaza CA, Blumenthal PD, Vogel H, Steinberg GK, Edwards MS, Li G, et al. Purification and characterization of progenitor and mature human astrocytes reveals transcriptional and functional differences with mouse. Neuron. 2016;89:37–53.
66. Mankhong S, Kim S, Moon S, Choi SH, Kwak HB, Park DH, Shah P, Lee PH, Yang SW, Kang JH. Circulating micro-RNAs differentially expressed in Korean Alzheimer's patients with brain abeta accumulation activate amyloidogenesis. J Gerontol A Biol Sci Med Sci. 2023;78:292–303.
67. Su L, Li R, Zhang Z, Liu J, Du J, Wei H. Identification of altered exosomal microRNAs and mRNAs in Alzheimer's disease. Ageing Res Rev. 2022;73:101497.
68. Ding Y, Chan CY, Lawrence CE. Sfold web server for statistical folding and rational design of nucleic acids. Nucleic Acids Res. 2004;32:W135-141.
69. Rennie W, Kanoria S, Liu C, Carmack CS, Lu J, Ding Y. Sfold tools for microRNA target prediction. New York: In Methods in Molecular Biology. Springer; 2019. p. 31–42.
70. Zhang J, Hou L, Zuo Z, Ji P, Zhang X, Xue Y, Zhao F. Comprehensive profiling of circular RNAs with nanopore sequencing and CIRI-long. Nat Biotechnol. 2021;39:836–45.
71. Xin R, Gao Y, Gao Y, Wang R, Kadash-Edmondson KE, Liu B, Wang Y, Lin L, Xing Y. isoCirc catalogs full-length circular RNA isoforms in human transcriptomes. Nature Communications. 2021;12:266.
72. Rahman MR, Islam T, Turanli B, Zaman T, Faruquee HM, Rahman MM, Mollah MNH, Nanda RK, Arga KY, Gov E, Moni MA. Network-based approach to identify molecular signatures and therapeutic agents in Alzheimer's disease. Comput Biol Chem. 2019;78:431–9.

73. Li S, Wang L, Fu B, Berman MA, Diallo A, Dorf ME. TRIM65 regulates microRNA activity by ubiquitination of TNRC6. Proc Natl Acad Sci U S A. 2014;111:6970–5.
74. Yao B, Li S, Jung HM, Lian SL, Abadal GX, Han F, Fritzler MJ, Chan EK. Divergent GW182 functional domains in the regulation of translational silencing. Nucleic Acids Res. 2011;39:2534–47.
75. Wang Y, Zhao J, Wu J, Liu J, Wang Y, Xu T, Zhang M, Zhuang M, Zou L, Sun W, et al. Genome-wide perturbations of A-to-I RNA editing dysregulated circular RNAs promoting the development of cervical cancer. Comput Biol Med. 2023;166: 107546.
76. Welden JR, Margvelani G, Arizaca Maquera KA, Gudlavalleti B, Miranda Sardon SC, Campos AR, Robil N, Lee DC, Hernandez AG, Wang WX, et al. RNA editing of microtubule-associated protein tau circular RNAs promotes their translation and tau tangle formation. Nucleic Acids Res. 2022;50:12979–96.
77. Arizaca Maquera KA, Welden JR, Margvelani G, Miranda Sardon SC, Hart S, Robil N, Hernandez AG, de la Grange P, Nelson PT, Stamm S. Alzheimer's disease pathogenetic progression is associated with changes in regulated retained introns and editing of circular RNAs. Front Mol Neurosci. 2023;16:1141079.
78. Shen H, An O, Ren X, Song Y, Tang SJ, Ke XY, Han J, Tay DJT, Ng VHE, Molias FB, et al. ADARs act as potent regulators of circular transcriptome in cancer. Nat Commun. 2022;13:1508.
79. Hondius DC, Koopmans F, Leistner C, Pita-Illobre D, Peferoen-Baert RM, Marbus F, Paliukhovich I, Li KW, Rozemuller AJM, Hoozemans JJM, Smit AB. The proteome of granulovacuolar degeneration and neurofibrillary tangles in Alzheimer's disease. Acta Neuropathol. 2021;141:341–58.
80. Fu XD, Ares M Jr. Context-dependent control of alternative splicing by RNA-binding proteins. Nat Rev Genet. 2014;15:689–701.
81. Li Y, Chen B, Zhao J, Li Q, Chen S, Guo T, Li Y, Lai H, Chen Z, Meng Z, et al. HNRNPL circularizes ARHGAP35 to produce an oncogenic protein. Adv Sci (Weinh). 2021;8:2001701.
82. Fei T, Chen YW, Xiao TF, Li W, Cato L, Zhang P, Cotter MB, Bowden M, Lis RT, Zhao SG, et al. Genome-wide CRISPR screen identifies HNRNPL as a prostate cancer dependency regulating RNA splicing. Proc Natl Acad Sci USA. 2017;114:E5207–15.
83. Olesnicky EC, Bono JM, Bell L, Schachtner LT, Lybecker MC. The RNA-binding protein caper is required for sensory neuron development in Drosophila melanogaster. Dev Dyn. 2017;246:610–24.
84. Olguin SL, Patel P, Buchanan CN, Dell'Orco M, Gardiner AS, Cole R, Vaughn LS, Sundararajan A, Mudge J, Allan AM, et al. KHSRP loss increases neuronal growth and synaptic transmission and alters memory consolidation through RNA stabilization. Commun Biol. 2022;5:672.
85. Carlyle BC, Kandigian SE, Kreuzer J, Das S, Trombetta BA, Kuo Y, Bennett DA, Schneider JA, Petyuk VA, Kitchen RR, et al. Synaptic proteins associated with cognitive performance and neuropathology in older humans revealed by multiplexed fractionated proteomics. Neurobiol Aging. 2021;105:99–114.
86. Zhu Y, Wang X, Forouzmand E, Jeong J, Qiao F, Sowd GA, Engelman AN, Xie X, Hertel KJ, Shi Y. Molecular mechanisms for CFIm-mediated regulation of mRNA alternative polyadenylation. Mol Cell. 2018;69(62–74): e64.
87. Andreone BJ, Larhammar M, Lewcock JW. Cell death and neurodegeneration. Cold Spring Harb Perspect Biol. 2020;12: a036434.
88. Okouchi M, Ekshyyan O, Maracine M, Aw TY. Neuronal apoptosis in neurodegeneration. Antioxid Redox Signal. 2007;9:1059–96.
89. Tixtha EJ, Super MK, Titus MB, Bono JM, Olesnicky EC. Roles for the RNA-Binding Protein Caper in Reproductive Output in Drosophila melanogaster. J Dev Biol. 2022;11.
90. Estfanous S, Daily KP, Eltobgy M, Deems NP, Anne MNK, Krause K, Badr A, Hamilton K, Carafice C, Hegazi A, et al. Elevated expression of MiR-17 in microglia of Alzheimer's disease patients abrogates autophagy-mediated amyloid-β degradation. Front Immunol. 2021;12:705581.
91. Pamudurti NR, Bartok O, Jens M, Ashwal-Fluss R, Stottmeister C, Ruhe L, Hanan M, Wyler E, Perez-Hernandez D, Ramberger E, et al. Translation of CircRNAs. Mol Cell. 2017;66(9–21): e27.
92. Yang Y, Fan X, Mao M, Song X, Wu P, Zhang Y, Jin Y, Yang Y, Chen LL, Wang Y, et al. Extensive translation of circular RNAs driven by N(6)-methyladenosine. Cell Res. 2017;27:626–41.
93. Chen CK, Cheng R, Demeter J, Chen J, Weingarten-Gabbay S, Jiang L, Snyder MP, Weissman JS, Segal E, Jackson PK, Chang HY. Structured elements drive extensive circular RNA translation. Mol Cell. 2021;81(4300–4318): e4313.
94. Wang F, Li Y. Identification of pathological pathways centered on circRNA dysregulation in association with irreversible progression of Alzheimer's disease. SRA. 2024; Available from: https://www.ncbi.nlm.nih.gov/bioproject/PRJNA992028
95. Wang F, Li Y. Identification of pathological pathways centered on circRNA dysregulation in association with irreversible progression of Alzheimer's disease. SRA. 2024; Available from: https://www.ncbi.nlm.nih.gov/bioproject/PRJNA1138662
96. Wang F, Li Y. Identification of pathological pathways centered on circRNA dysregulation in association with irreversible progression of Alzheimer's disease. SRA. 2024; Available from: https://www.ncbi.nlm.nih.gov/bioproject/PRJNA1138661
97. Wang F, Li Y. YaoLabEmory/ADcircRNA. GitHub. 2024. Available from: https://github.com/YaoLabEmory/ADcircRNA.

Publisher's Note